e-Newsletter n°2

May 2006
Published twice a year
Available at http://www.bright-eu.org

WWW.BRIGHT.EU

*Wide Wavelength light for public Welfare: High-**Brig**htness Laser Diode Systems for **H**ealth, **T**elecom and **E**nvironment **U**se*

WWW.BRIGHT.EU is an integrated project supported by the European Commission's Information Society Technologies programme

CONTENT

EDITORIAL

Welcome to the second Newsletter of the integrated project WWW.BRIGHT.EU, which started in July 2004.
If you wish to find out more about our project or would like to read our first Newsletter, please visit our website:
http://www.bright-eu.org/
We hope you will enjoy the reading.

The Editors

Myriam Oudart
Alcatel Thales III-V lab
myriam.oudart@3-5lab.fr

Eric Larkins
University of Nottingham
Eric.Larkins@Nottingham.ac.uk

GREETINGS FROM THE PROJECT COORDINATOR

Michel Krakowski
Project Coordinator
Alcatel Thales III/V Lab
Route départementale 128
91767 Palaiseau
FRANCE
michel.krakowski@3-5lab.fr

Dear Reader,

Welcome to the second e-Newsletter of the IST Project WWW.BRIGHT.EU: Wide Wavelength light for public Welfare High-Brightness Laser Diode Systems for Health, Telecom and Environment Use, a European Integrated Project on high-brightness laser diode technologies. Indeed, **High brightness laser diode technology** is a key enabling technology for the information society of tomorrow, especially in the fields of **health-care, telecommunication, environment and security**.

The WWW.BRIGHT.EU consortium of 23 partners is pursuing a long-term vision aimed at pushing the limits of the current laser diode technology towards higher brightness, and stimulating the development of new applications and markets such as biophotonics (photodynamic therapy and fluorescence diagnosis). Our approach consists of mobilising the expertise of the main European actors of the laser diode core technology, and coupling it with highly innovative optical technologies. Industrialisation issues are being explored through packaging and reliability studies.

Our project is going well. A lot of good results have been obtained as shown by the important list of publications and conference papers listed in this Newsletter. There are strong interactions and regular and various exchanges between partners. This second Newsletter gives the project news and presents three technical topics: quantum dot material, modelling of tapered lasers and micro-optics for coupling into fibres among the several ones covered by our project.

We hope that you find our e-Newsletter interesting and informative. If you are interested in exploring the advantages offered by high-brightness lasers for your applications or simply wish to comment upon or discuss any of the issues touched upon in the e-Newsletter in greater depth, please do not hesitate to contact us.

An introduction to environmental toxicology

By Nicole PROUST, Clean technology expert, TRT-Fr

Before reviewing the hazards and the risks for operators related to III-V MOCVD, it is necessary to explain briefly how chemicals can interact with biological cells in order to introduce environmental toxicology.

1- Toxicology in brief

After exposure to xenobiotics (foreign substances), the objective of the organism is to transform these exogen chemicals into water-soluble metabolites (by-products) easily excretable - generally through urine.
The solubility is of importance as the starting chemical or its metabolites can exhibit different characteristics: soluble in water, in lipid, in both or insoluble.
Chemicals can enter the human organism by several routes, the most important are the respiratory, the nasal, the cutaneous and the oral ones, the oral being a secondary one. [Hugues, 1996]

The respiratory track is composed of three different specific regions, which prohibit or limit the ability of toxins to enter.
In the upper part of the respiratory tract, from nostrils to larynx, the air is cleaned, humidified and thermally adjusted. Mucus and hairs are able to trap particulates larger than 5 µm in diameter preventing them from entering the lower part of the respiratory system.
The tracheobronchial region is composed of the trachea, the bronchi and the bronchioles. A mucociliar escalator can trap small particulates (2-5 µm) and water-soluble toxic gases, which will be transported out of the lower region of the respiratory system.

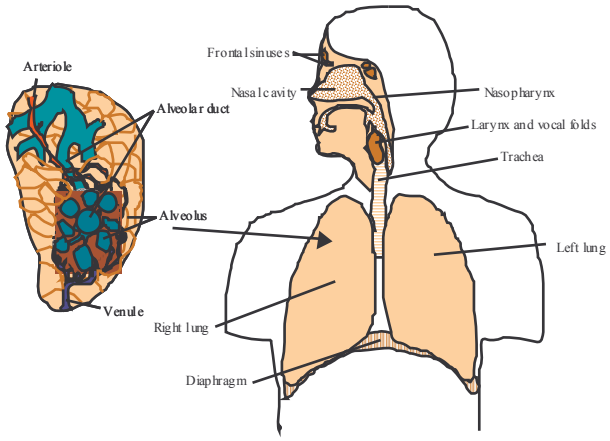

Respiratory system route

The final part is the alveolar region, where respiration takes place. The end result is 400- 1200 millions alveoli in a healthy adult human lung, which means a surface area of approximately 80 - 120 m^2 for gas exchange. Particulates of less than 1 µm as well as non-water-soluble gases can reach the alveoli. Then, before the initial pollutant may enter the cardiovascular system, different biological processes will take place according to the nature of the pollutant and properties.
The amount of toxin that can enter the body is a function of the volume breathed in one minute. This volume for a normal adult at rest is in the range of 6 litres, this value is very significantly enhanced under physical activity and this allows increased contact of the pollutant with the alveoli tissue. Due to the specificity of the respiratory tract and its close association with the blood stream, pneumocytes (cells which form the alveoli) are able to transport the toxins quickly in the lung blood circulation for a distribution in the rest of the organism.

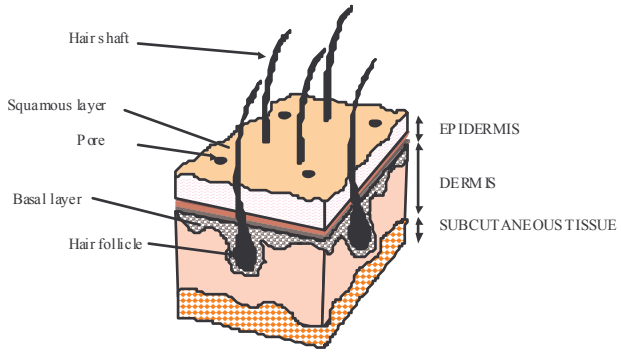

Structure of human skin

Several routes of absorption through the skin are possible; the most common is the cutaneous adsorption followed by a passive diffusion through the epidermis into the dermis, where the xenobiotics may enter a blood vessel. If the exogen chemical enters a hair follicle or a sweat gland, the passage into the derm will be accelerated.
Molecules small in size, non-polar and lipid-soluble will diffuse quickly.
Skin burns enhance penetration and distribution of toxins into the organism.

The digestive route from mouth, to stomach and intestines, also includes organs such as pancreas and liver… Absorption can take place across the mucosal lining anywhere along the digestive system.
Most of the absorption of food and toxins takes place in the small intestine, while the large intestine, which is the final region of the digestive system, is not considered a major site of absorption for occupational xenobiotics.

There is a significant difference between the pulmonary and the oral routes in terms of metabolisation. In brief, the toxin may go directly into the circulatory system when exposure occurs by the pulmonary route. In the case of ingestion, the toxin may go first through the liver before passing into the blood stream. The liver acts as a filter, since many of the biological processes of metabolisation and detoxification take place here.

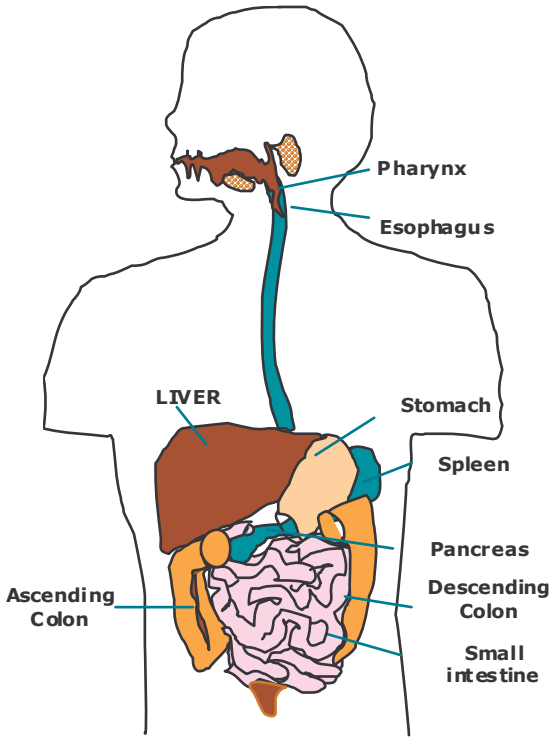

Digestive system route

After exposure, absorption will occur. Absorption is the process by which toxins cross the epithelial biological cell barrier. Depending on a lot of factors (nature of the chemical, dose, duration and type of exposure), the toxin may limit its contact with the outer surface of the cell or cross the cell barrier, enter into the cell, move through the cell, enter into the circulatory or lymphatic system.
To enter into a cell, chemicals have to diffuse through its lipidic membrane, which is easy for lipid-soluble substances. Xenobiotics when in the blood stream may be transformed and are disseminated into the organism. Some biological transformations take place in various organs (liver, kidney…); tissues (skin….) or blood and by-products are created. The various reactions of metabolisation are more or less sophisticated, sometimes they can they can take time, particularly for lipid-soluble substances. Such specie, during their "travel" into the organism, will stay and be stored in some organs for a variable period of time, from hours to years depending on the chemical molecule. This results in more or less important toxicity problems. The figure below summarises the situation from exposure to intoxication and excretion.
The liver is a very important organ that acts as a filtering system. Many xenobiotic chemical metabolisation reactions take place into this filter and its role is important for arsenic.

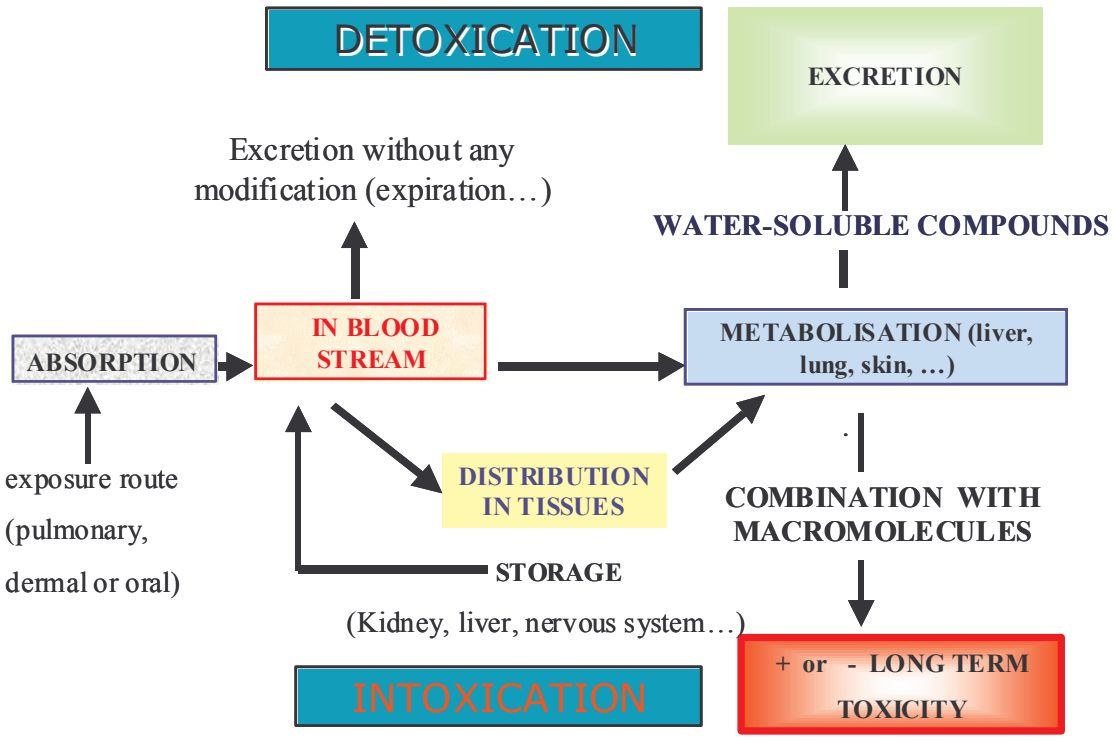

From exposure to intoxication and excretion

2- Important properties of chemicals

Some physicochemical properties of chemical species are very important because they give useful information to try to understand toxicity mechanisms. The physical state of the molecule at room temperature, the melting and boiling temperature, the solubility… are some parameters that help to evaluate the way of penetration and the magnitude of the potential exposure. Reactivity with water, dioxygen and others is also important. We have to keep in mind that water is one of the preponderant constitutive components of biological environments (75 %) and some toxins will interact with this ubiquitous molecule. Chemical solubility determines the penetration kinetics into the cells and then the metabolisation and excretion kinetics. The figure opposite illustrates the influence of solubility on the metabolisation pathway. As indicated above, toxic molecules can be insoluble, lipid-soluble or water-soluble. Sometimes chemicals have a partition coefficient between water and lipids, which complicates the situation, but is very important. Absorption, repartition and storage of an element in the organism depend on the chemical species concerned (speciation) and are a function of the specific compound.

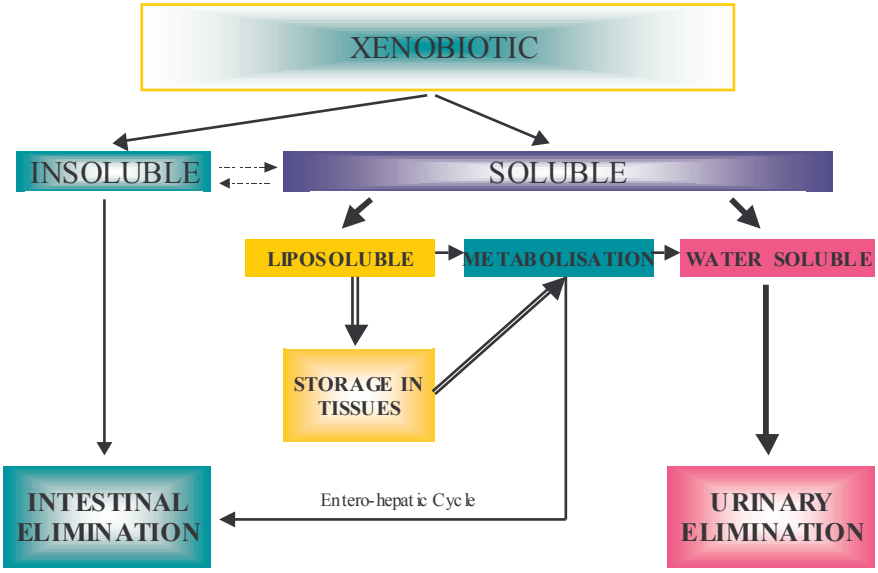

Influence of solubility on the metabolisation pathway

In summary, the toxicity of ions and molecules depends on their physicochemical properties at ambient temperature, volatility, solubility in water and/or in lipids, reactivity with di-oxygen, possibility to form organomineral compounds... This first part is a brief introduction to environmental toxicology, it will be followed by other parts giving information on arsenic, gallium and indium toxicity and on risks related to III-V MOCVD (see the next e-Newsletter).

Bibliography

Hugues W. W., Essentials of Environmental Toxicology : the effects of environmentally hazardous substances on Human health, 1996, Taylor and Francis, London.

RECENT PUBLICATIONS

- S. Bull, J.W. Tomm, M. Oudart, J. Nagle, C. Scholz, K. Boucke, I. Harrison, and E.C. Larkins, "By-emitter degradation analysis of high power laser bars," J. Appl. Phys, Sept 2005.
- S. Bull, A.V. Andrianov, I. Harrison, R. Kerr, M. Dorin, J. Noto, and E.C. Larkins, "Development of a spectroscopically resolved photo- and electroluminescence microscopy technique for advanced studies of high power and high-brightness laser diodes," IEEE Trans. Instrum. Meas., 54, pp. 1079-1088, 2005.
- Jens W. Tomm, Mark L. Biermann, B. S. Passmore, M. O. Manasreh, A. Gerhardt and Tran Q. Tien, "Spectroscopic analysis of external stresses in semiconductor quantum-well materials," Mater. Res. Soc. Symp. Proc. 829, 233-242 (2005).
- Tran Quoc Tien, Jens W. Tomm, Myriam Oudart and Julien Nagle, "Mechanical strain and defect distributions in GaAs-based diode lasers monitored during operation," Appl. Phys. Lett. 86, 111908, 1-3 (2005).
- Tran Quoc Tien, Axel Gerhardt, Sandy Schwirzke-Schaaf, Jens W. Tomm, Holger Müntz, Jens Biesenbach, Myriam Oudart, Julien Nagle, and Mark L. Biermann, "Relaxation of packaging-induced strains in AlGaAs-based high-power diode laser arrays," Appl. Phys. Lett. 86, 101911, 1-3 (2005).
- J. W. Tomm, A. Gerhardt, M. L. Biermann, and J. P. Holland "Quantitative spectroscopic strain analysis of AlGaAs-based high-power diode laser devices," Eur. Phys. J. Appl. Phys 27, 461-464 (2004).
- A. Gerhardt, J. W. Tomm, M. Oudart, Y. Sainte-Marie, and J. Nagle "Simultaneous quantitative determination of strain and defect profiles within the active region along high-power diode laser bars by micro-photocurrent mapping," Eur. Phys. J. Appl. Phys. 27, 451-454 (2004).
- Jens W. Tomm, Fritz Weik, Axel Gerhardt, Tien Quoc Tran, Jens Biesenbach, Holger Müntz, and Gabriele Seibold "Transient thermal tuning properties of single emitters in actively cooled high-power cm-bar arrays," SPIE Proc. 5336, 125-131 (2004).
- Axel Gerhardt, Fritz Weik, Tien QuocTran, Jens W. Tomm, Thomas Elsaesser, Jens Biesenbach, Holger Müntz, Gabriele Seibold, and Mark L. Biermann "Device deformation during low-frequency pulsed operation of high-power diode bars," Appl. Phys. Lett. 84, 3525-3527 (2004).
- Mark L. Biermann, Steven Duran, Kelsey Peterson, Axel Gerhardt, Jens W. Tomm, Witold Trzeciakowski, and Artem Bercha "A general, spectroscopically-based method of quantitative strain analysis in semiconductor, quantum-well devices," J. Appl. Phys. 96, 4056-4065 (2004).
- Anna Kozlowska and Mateusz Latoszek, Jens W. Tomm, Fritz Weik, Thomas Elsaesser, Mariusz Zbroszczyk, Maciej Bugajski, B. Spellenberg and M. Bassler "Analysis of thermal images from diode lasers Temperature profiling and reliability screening," Appl. Phys. Lett. 86, 203503, 1-3 (2005).
- Anna Kozlowska, Fritz Weik, Jens W. Tomm, Andrzej Malag, Mateusz Latoszek, Piotr Wawrzyniak, Marian Teodorczyk, Lech Dobrzanski, Mariusz Zbroszczyk, Maciej Bugajski "Thermal properties of high-power diode lasers investigated by micro-thermography," SPIE Proc. 5711, 158-165 (2005).
- A. Bercha, F. Dybala, K. Komorowska, P. Adamiec, R. Bohdan, W. Trzeciakowski, J.A. Gupta, P.J. Barrios, G. Pakulski, A. Delage, and Z.R. Wasilewski, "Pressure tuning of GaInNAs laser diodes in external cavity," Proceedings of SPIE -- Volume 5722 Physics and Simulation of Optoelectronic Devices XIII, Marek Osinski, Fritz Henneberger, Hiroshi Amano, Editors, April 2005, pp. 565-572

- E. Samsøe, P. M. Petersen, S. Andersson-Engels and P. E. Andersen, "Second harmonic generation of 405 nm light using periodically poled KTiOPO4 pumped by external-cavity laser diode with double grating feedback," Appl. Phys. B, 80(2005), pp. 861-4.
- P. M.Petersen, E. Samsøe, S. Blaabjerg and P. E. Andersen, "Guiding of laser modes based on self-pumped four-wave mixing in a semiconductor amplifier," OPTICS EXPRESS 13(2005), pp. 3340-7.
- M. Chi, B. Thestrup and P. M. Petersen, "Self-injection locking of an extraordinarily wide broad-area diode laser with a 1000-nm wide emitter," Opt.Lett. 30(2005), pp. 1147-9.
- N. Kjaergaard, E. Samsoe, H. Lausen, P. E. Andersen and P. M. Petersen, "An external-cavity laser diode at 635 nm for laser display applications," Opt. Commun. 245(2005), pp. 333-9
- M. Chi, O. B. Jensen, J. Holm, Chr. Pedersen, P. E. Andersen, G. Erbert, B. Sumpf, P. M. Petersen, "Tunable high-power narrow-linewidth semiconductor laser based on an external-cavity tapered amplifier", Optics Express Vol. 13, No. 26; 10589 – 10596 (2005)

- J.M.G.Tijero, D.Rodríguez, L.Borruel, S.Sujecki, E.C.Larkins and I.Esquivias, "Optimization of epitaxial layer design for high brightness tapered lasers."Proceedings SPIE 5722
- A. Knauer, G. Erbert, R. Staske, B. Sumpf, H. Wenzel and M. Weyers, "High-power 808-nm lasers with a super-large optical cavity," Semicond. Sci. Technol. 20, 621-624 (2005)
- Marc T. Kelemen, Juergen Weber, Michael Mikulla and Guenter Weimann, "High-Power High-Brightness Tapered Diode Lasers and Amplifiers," Proceedings SPIE 5723, p. 29.
- B. Sumpf, M. Zorn, R. Staske, J. Fricke, P. Ressel, G. Erbert, M. Weyers, G. Tränkle, "High-efficient 650 nm laser bars with an output power of about 10 W and a wall-plug efficiency of 30%", Photonics West – Novel In-Plane Semiconductor Lasers - 21 - 26 January 2006; San Jose, California; USA – Paper 6133-14
- M.T. Kelemen, J. Weber, G. Kaufel, G. Bihlmann, R. Moritz, M. Mikulla and G. Weimann, "Tapered diode lasers at 976 nm with 8 W nearly diffraction limited output power," Electronics Letters, UK * vol 41 (1 Sept 2005), n°18, p 1011-13
- M.T. Kelemen, J. Weber, G. Kaufel, R. Moritz, M. Mikulla, and G. Weimann, "8 W high-efficiency high-brightness tapered diode lasers at 976 nm", SPIE Proc. 6104, paper 13, 2006
- N. Michel, M. Calligaro, M. Krakowski, S. Deubert, H.P. Reithmaier, A. Forchel, "Lasers évasés guidés par l'indice à 980 nm, de forte brillance (1 W CW, M2 = 2.9) à boîtes quantiques en GaInAs/(Al)GaAs," 23èmes Journées Nationales d'Optique Guidée 2004 (JNOG 2004), Paris, 25-27 octobre 2004, Recueil des Communications, édité par la Société Française d'Optique, pp. 43-45.
- N. Michel, M. Calligaro, M. Krakowski, S. Deubert, J.-P. Reithmaier, and A. Forchel, "980 nm small aperture tapered laser (1W CW, M2~3) and tapered arrays (>3W CW): comparison between GaInAs/(Al)GaAs quantum dot and quantum well structures," Proc. SPIE Vol. 5738, pp. 355-364 22-27 January 2005, San Jose (USA).
- N. Michel, M. Krakowski, M. Calligaro, M. Lecomte, O. Parillaud, L. Borruel, I. Esquivias, P. Moreno, S. Sujecki, J. Wykes and E.C. Larkins, "High-power and high-brightness lasers with an Al-free active region at 915 nm," (ECOC 2005), Glasgow, Scotland, 25-29 September 2005.
- S. Deubert, R. Debusmann, J.P. Reithmaier and A. Forchel, "High Power 915 nm QD lasers with improved temperature stability of the emission wavelength for uncooled pump applications," Electronics Letters 41, 1125 (2005)

- Dominique Bayart, "Prospects for Cladding-Pumped Erbium-Doped Fiber Amplifiers (CP-EDFA)," Proceedings of European Conference on Optical Communication, ECOC 2004, Stockholm, Sweden, pp. 348-51.

- S. Andersson-Engels, K. Svanberg and S. Svanberg, "Fluorescence imaging in medical diagnostics," book chapter in Biomedical Optics. 2005 (in press).
- C. af Klinteberg, M. Andreasson, O. Sandström, S. Andersson-Engels and S. Svanberg, "Compact medical fluorosensor for minimally invasive tissue characterisation," Rev Sci Instrum 76(2005).
- J. Swartling, J. Svensson, D. Bengtsson, K. Terike and S. Andersson-Engels, "Fluorescence spectra provide information on the depth of fluorescent lesions in tissue," Appl Opt 44(2005), 1934-41.
- D. Gorpas, C. Politopoulos, E. Alexandratou, M. Kyriazi and D. Yova, "A Binocular Machine Vision System for Non Melanoma Skin Cancer 3D Reconstruction", SPIE Photonics West, BiOS 06, San Jose, California, USA
- E. Alexandratou, M. Kyriazi, D. Yova, S. Gräfe, T. Trebst, A. Johansson, J. Svensson, K. Svanberg, N. Bendsoe, S. Anderson-Engels, "A Distribution studies of m-THPC after topical application of m-THPC thermogel in a murine non-melanoma skin cancer tumor model by fluorescence spectroscopic and imaging techniques", SPIE, vol. 6139, Optical methods for tumor treatment and detection: Mechanisms and techniques in photodynamic therapy, 2006.

PRESENTATIONS OF SOME OF THE PARTNERS

Partner 14- Lund Laser Centre

Lund Laser Centre (LLC) is located within Lund University in Sweden and specializes in exploring light-matter interaction both for basic research and for a large number of applications. Being one of the largest laser laboratories in Northern Europe, it is included in the European Commission Large Scale Infrastructure programme, meaning that any researcher within EU can apply to utilize this laboratory for projects requiring unique equipment or expertise available at LLC. Information about the facilities and the application procedure is available through the home-page: www.llc.lth.se.

Lund University also hosts a Medical Laser Centre as an active part of the Lund Laser Centre. This Centre is headed by Prof. Stefan Andersson-Engels from Department of Physics and Associate Professor Katarina Svanberg from Department of Oncology. These persons also lead the LLC activities within the Bright project. The research at the Centre is within the field of biomedical optics with clinical applications. We have been working with methods to measure optical properties, both for diagnostic purposes and for dosimetry in connection to photodynamic therapy. The expertise gained in modeling and measurements of optical properties has been used to develop a novel interstitial photodynamic system with on-line feedback. Spectroscopy is here used to reveal the presence of important constituents for PDT during the treatment: light, photosensitizer and oxygen. For these measurements, we have also employed the long experience of fluorescence spectroscopy for tissue diagnostics, another main area of research within the Centre, with numerous clinical evaluation studies with positive results. Much effort has also been paid to develop tools for time-resolved diffuse remittance spectroscopy to measure absorption and scattering spectra. Developed instruments and evaluation routines have been used in optical mammography research and have also gained interest for in-line control measurement in the pharmaceutical industry. The development of a novel technique to measure the absorption of a gas in highly scattering materials has been successful. This technique has been explored for monitoring the sinus cavities. Another direction of the research at the Centre has been to develop novel laser- based X-ray sources for radiographic imaging, where the small source size and possibilities for gated imaging suppressing scattered X-rays, provide interesting prospects in reduced absorbed dose.

The Centre has contributed significantly to the field of biomedical optics. Historically, the group has been a pioneer in both fluorescence spectroscopy and time-resolved remittance measurements for tissue diagnostics, as well as in photodynamic therapy using topically applied ALA for photosensitization.

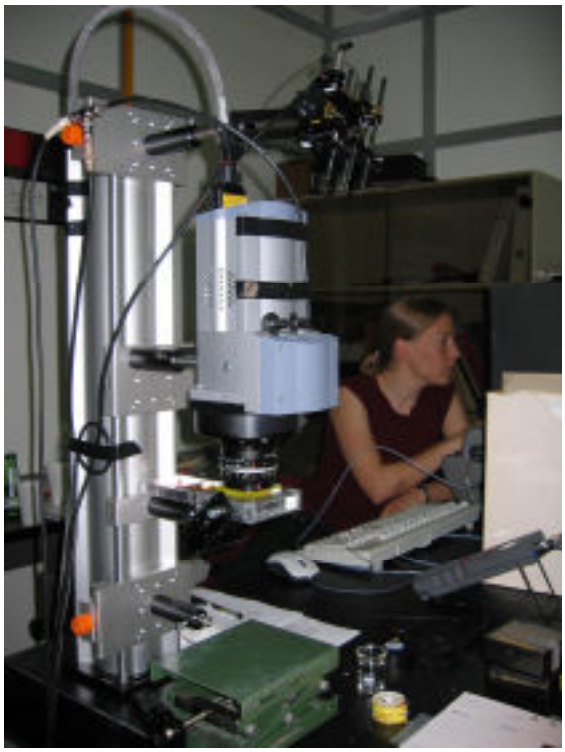

The research interest of the group has since expanded both on the basic research level and on clinical applications. During recent years, the most outstanding research activities involve clinical evaluation of fluo-rescence spectroscopy and imaging in a number of clinical specialities, development of a system for interstitial photodynamic therapy utilizing results from on-line feed-back measurements for treatment guidance, tissue characterization using time-resolved spectroscopy, as well as the development of a technique to measure concentration of gases in turbid media, such as tissue.

The ongoing research and development in photodynamic therapy yields a possibility to treat larger tumour volumes and may thus allow inclusion of new indications to be treated. Presently, a pilot clinical study for treatment of malignant lesions in the prostatic gland is planned. Clinical fluorescence spectroscopy/ imaging studies have been conducted to evaluate the potential of the technique in characterizing colonic polyps as well as laryngeal and brain tumours with very good results. Fluorescence techniques are also refined to enable improved depth resolution in fluorescence molecular imaging. We have furthermore pursued time-resolved measurements for tissue charac-terization, by, for instance, developing a system based on white-light generation in a micro-structured optical fibre, and detection of the remitted broad-band light with both wavelength and temporal resolution using a spectrometer equipped with a streak-camera. The time-resolved technique has been used for characterizing breast tissue *in vivo*, and has also led to a spin-off project, where AstraZeneca are very interested in developing a technique for inline production analysis of pharmaceuticals. The aim with another project within the group is to employ the unique features of the GASMAS technique developed within the group for specific clinical problems. Here sinus cavity diagnostics is a first application. Premature / Neonatal lung diagnostics is a further possibility to explore.

Activities in WWW.BRIGHT-EU

The research activities within the BRIGHT.EU project is concentrated to the development and evaluation of pulsed 405 nm diode lasers for fluorescence diagnostics. The partner has already participated in two joint measurement campaigns within the biomedical application workpackage; one at ICCS in Athens and one at Biolitec in Jena.

For further information, please contact Prof. Stefan Andersson-Engels, tel: +46-46-2223121 (Stefan.andersson-engels@fysik. lth.se).

Partner 20- The University of Nottingham

The Photonic and Radio Frequency Engineering Group (PRFEG) in the School of Electrical and Electronic Engineering pursues cutting edge research topics in photonics and microwave technology. PRFEG researchers have come together from a wide range of cultural backgrounds to create a dynamic and enthusiastic research environment. The group's research activities are organised along three research strands, which are funded by the European Commission, EPSRC and industry.

The research activities of the High-Power Optoelectronics research strand, established in 1995, have contributed to the European high-power laser diode projects WWW.BRIGHT.EU, POWERPACK, ULTRABRIGHT and also NODELASE. The group's activities focus on: a) the design and modelling of high-power and high-brightness lasers; b) reliability and degradation studies of high-power laser diodes; and c) the development of novel high-brightness laser diodes.

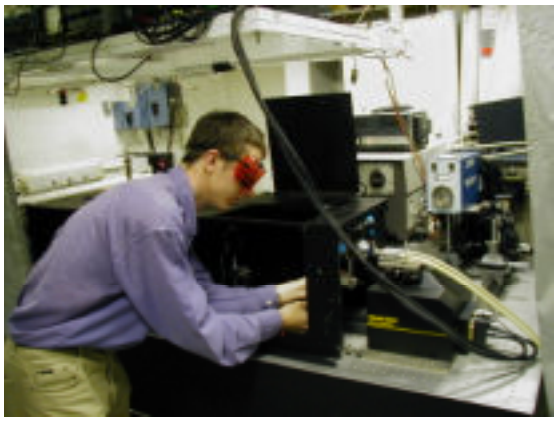

Mounting a laser bar for a spectroscopic electroluminescence microscopy measurement

The Group has successfully developed 2.5D & 3D coupled models (i.e. optical, electronic and thermal), including a multi-wavelength "spectral" model for the predictive design and simulation of high-brightness laser diodes.

Advanced models for gain dynamics and thermal effects in laser diodes are also being developed. We have developed a high-current (50A) non-destructive probe for CW testing of unmounted laser bars and a flexible, state-of-the-art facility for characterising optoelectronic materials and devices. Recently, we proposed a "by-emitter" degradation analysis method, which allowed us to identify a packaging-induced strain threshold for emitter degradation.

The research activities of the Photonic Communications Technology research strand are focused on studying devices, physical effects and materials that will have a major impact on communications infrastructure over the next decade. These include gain dynamics and non-linear optical effects in semiconductor optical amplifiers (SOAs) for wavelength conversion and functional photonics, novel optical materials and optical power budget / amplification in photonic integrated circuits (PICs). A particular emphasis is given to optical sampling using SOA-based four wave mixing for pulse characterisation and bit error rate (BER) estimation. Optical regeneration technologies and optical performance monitoring techniques are also being investigated. Furthermore, there is an activity looking at the non-linear effects of real components in optical network / system contexts including the transmission of rf signals over optical communication channels.

The RF Devices, Circuits and Materials research strand activities, grew out of a close interaction with the School of Physics. The activities are more oriented towards the interaction of microwaves with materials in general as well as the design of microwave integrated circuits for material assessment applications. In collaboration with the applied optics group, we are investigating active pixel circuits operating above 1GHz. Devices for microwave power and millimetre waves are being actively investigated. The strand is benefiting from the purchase of a new vector network analyser that will allow the characterization of active and passive rf devices and circuits to 330 GHz.

PRFEG belongs to the University of Nottingham Institute of Materials (UNIMAT) and plays a leading role in the UNIMAT Interdisciplinary Doctoral Training Centre (IDTC) for Photonics and Electronics, which is funded by the University to stimulate interdisciplinary research and training between the Schools of Electrical and Electronic Engineering, Physics, Chemistry, Mechanical, Materials and Manufacturing Engineering, Pharmacy, and Medical and Surgical Sciences.

The IDTC promotes interdisciplinary research and the training of interdisciplinary researchers.

Activities in WWW.BRIGHT-EU

Within the project, UNott are contributing in the areas of laser simulation and design, advanced characterisation, and reliability. UNott are developing a new spectral laser simulation tool for the simulation of high-brightness external cavity laser diodes and are also working with UPM on the simulation and design optimisation of tapered lasers. UNott is performing detailed intracavity electroluminescence imaging measurements on tapered lasers, which will be used for advanced validation of the laser simulation tools. UNott is using the by-emitter technique to look at bar-level degradation processes due to thermal, electrical and mechanical interactions between emitters. Spectroscopically-resolved photoluminescence microscopy measurements are being used to investigate correlations between degradation and the distribution of strain. Finally, UNott are also co-ordinating the WWW.BRIGHT.EU training and dissemination activities.

For further information, please contact: Professor Eric Larkins (eric.larkins@nottingham.ac.uk) Tel: +44 115 951 5534.

Partner 22- University of Würzburg

Overall presentation

Microstructure Laboratory of the Technische Physik with 550 m² clean room.

The group at Würzburg University is investigating different III-V material systems and new concepts for the development of opto-electronic devices. Based on high-resolution lithographic systems, nanostructure patterning techniques with minimum feature sizes below 10 nm were developed for opto-electronic applications as well as for basic physics studies. The Microfabrication Laboratory of the group (550 m² cleanroom) includes solid source and gas source MBE systems for different III-V material systems, high resolution electron beam lithography, a high resolution focused ion beam system, different dry etching systems, cw-, pulsed and high frequency measurement tools for opto-electronic devices. For basic material studies e.g. high-Q cavities high resolution photo-luminescence setups are available. Also, transport properties of nano-structured electronic devices are investigated. Based on molecular beam epitaxy, low threshold, high efficiency quantum well and quantum dot laser structures were developed for high power and telecommunication applications.

Based on different material systems (GaAs, InP, GaSb), we cover the whole wavelength range from about 0.8 to 2.7 µm. Record values in cw output powers of quantum dot lasers of 6.3 W were achieved at 980 nm. Quantum dot lasers for 1.3 µm emission wavelengths were realized with high device performance (e.g. Ith = 2 mA for 400 µm long device) and for longer wavelength applications quantum dash structures were developed on InP substrates with transparency current densities < 500 A/cm2 and emission wavelengths in the range between 1.4 to 2 µm. Ridge waveguide lasers achieved threshold currents below 20 mA at room temperature (300 µm long device). The first room temperature lasers worldwide emitting > 1.5 µm on GaAs using nitride-containing layers were reported in 2000. Also research activities on quantum cascade lasers for mid and far infra-red on GaAs and on InP are performed within the group.

By using high-resolution lateral patterning techniques (electron and focused ion beam lithography), complex-coupled DFB lasers with first order gratings were developed for telecommunication and sensor applications in different material systems and for different wavelength ranges (0.8 - 1 µm, 1.3 µm, 1.55 µm and > 2 µm). Devices in the 1.55 µm wavelength range were developed for high speed applications. High frequency operation up to 22 GHz has been achieved on high performance single mode lasers.

New design concepts were developed based on multi-section structures, which allow a strong enhancement of the high frequency properties. Up to 37 GHz small signal modulation bandwidth was demonstrated. Another major research activity is the fabrication and characterization of photonic crystal structures, which require both high resolution E-beam and dry etching techniques. This approach requires the development of etch processes with high aspect ratios, smooth sidewalls and excellent geometry control. A number of novel opto-electronic devices (e.g. PC based lasers) as well as structures for fundamental studies of photonic crystals have been realized with this technology.

The major devices and device concepts have been developed within the frame of different national and European projects in cooperation with large industrial partners (e.g. Infineon, Alcatel, Thales …) and different medium and small size companies.

The research group was and is active as coordinator and partner in different EU projects (e.g. NANOPT, NANOLASE, Q-SWITCH, PCIC, ULTRABRIGHT, NANO-TCAD, BIGBAND; FUNFOX, ZODIAC, WWW. BRIGHT-EU, …).

Activities in WWW.BRIGHT-EU

Within the project, the group at Würzburg University is realizing quantum dot laser structures at 915 nm for uncooled pump applications.

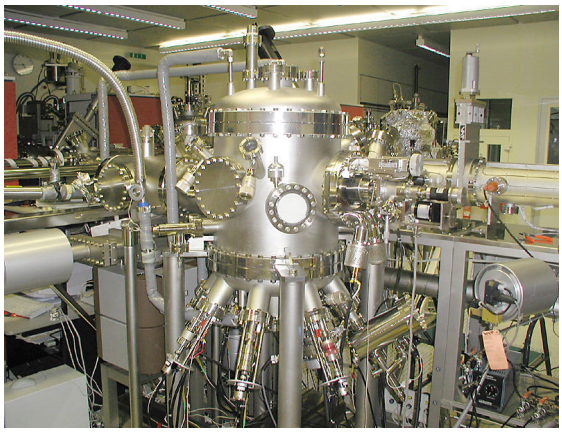

Molecular Beam Epitaxy machine for GaAs inside the Microstructure Laboratory.

The goal is to make use of the improved temperature stability of the emission wavelength of the quantum dots to achieve a thermal induced wavelength shift lower than 0.1 nm/K. From these structures, tapered lasers are processed to investigate the capability of quantum dots in uncooled pump modules. Another task is the implementation of lateral gratings on tapered lasers for wavelength stabilization and multiplexing. The aim within this project is to achieve more than 1 W of single mode output power from a 915 nm quantum dot laser.

Partner 21- Universidad Politécnica de Madrid (UPM)

The Universidad Politécnica de Madrid (Technical University of Madrid) is the largest academic institution in Spain devoted to education and research in engineering and applied sciences. Its more than 4000 faculty staff personnel and PhD students participate in research and development projects founded by local, national and European institutions both public and private. Since 1998 UPM is one of the most active European institutions in the EU Framework Programs: it participated in 162 projects of FP5 with a total funding of around 24 M€. At present, it is involved in 56 projects in the FP6 in different thematic priorities.

UPM is participating in WWW.BRIGHTEU through the "Applied Photonic Group" at the "Departamento de Tecnología Fotónica" (Photonic Technology Dept.). The group started its activity in semiconductor lasers in 1992 and since then it has conducted research in this activity in different European projects (NODELASE 1996-99, ULTRABRIGHT 2000-03, WWW.BRIGHT.EU 2004-06) and national projects in collaboration with international and national groups. The main research fields of the group in the last years have been: modelling of high speed laser dynamics, including carrier capture and escape balance, new techniques for laser diode characterisation (Capacitance–Voltage, sub-threshold Power-Current -Voltage measurements, spatially resolved spectral analysis, gain and linewidth enhancement factor measurements), modelling of high brightness tapered lasers, and modelling and applications of VCSELs.

The group has published more than 100 journal and conference papers on laser diodes, and has developed and registered a software program for the simulation of High Power Lasers (HAROLD 3.0) which is currently under commercial exploitation.

Activities in WWW.BRIGHT-EU

The activity of UPM in the project consists of the modelling, simulation and design of optimised tapered lasers emitting at several wavelengths in the near infrared. The final goals of this activity are twofold. The first goal is to provide the fabricating partners with design recommendations of tapered lasers with optimised brightness.

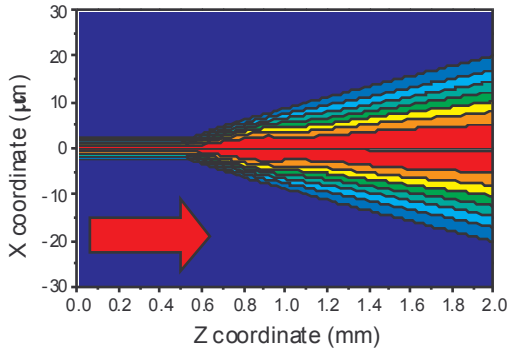

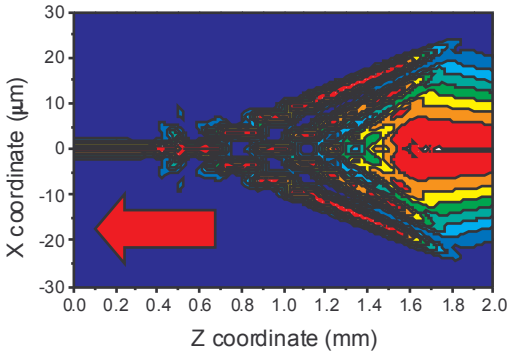

Simulation of the normalised forward (top) and backward (bottom) field intensity profile of an index guided tapered laser.

The second goal is to gain, based on simulations, an understanding of the underlying physics that determines the behaviour of the devices, which will help in the optimisation of the design.

UPM and UNott in a collaborative work have developed a steady state simulation tool (ILDSP) in the framework of a previous project (ULTRA-BRIGHT), that has demonstrated to be able to predict the behaviour of several tapered lasers. A first task of UPM in the project is to simulate with the ILDSP tapered lasers at 975 nm and 915 nm with different geometries and different epitaxial layer structures to seek an optimised design. A second task, in collaboration with UNott, is the upgrading of ILDSP by incorporating capabilities for the simulation of lasers with new geometries (built-in lenses, curved mirrors). Finally, a third task (also in collaboration with UNott) is to use the upgraded tool to perform simulations and provide the fabricating partners with design recommendations for the new devices.

For further information please contact: Professor Ignacio Esquivias Tel: +34913367339. (esquivia@tfo.upm.es)

Consortium of WWW.BRIGHT.EU

Micro-optic cylindrical aspheric laser collimator for high power diode lasers

Authors: M. Forrer, E. Langenbach, M. Meeder, D. Kura, FISBA OPTIK AG, Switzerland

Update: 31.1.06

FISBA OPTIK AG

FISBA OPTIK AG is a company based in St. Gallen, Switzerland, with around 370 employees, specialising in high quality optics and optical systems for high-tech applications. Featured products are high power diode laser systems, camera objectives and interferometers. Areas of expertise with respect to BRIGHT.EU are micro-optics design and fabrication, specific laser coatings, micro-optics packaging, high-brightness laser module assembly and system integration. The optical design, the development and the in house production of optical and optoelectronic systems based on diode lasers is the basis for many successful OEM-products in diverse application areas, such as industrial printing, industrial plastic welding and soldering, medicine, defence and aerospace.

High power diode laser collimation lens

Fast-axis aspheric laser collimators have found numerous applications in high-power diode laser systems. The laser radiation is used indirectly as a pump source for solid-state laser systems as well as for direct applications of the laser-diode emission in industrial processing, defence, space and for medicine. High-power diode lasers will continue to economically penetrate application fields traditionally occupied by conventional laser systems, with more than several Watts available from a single diode laser emitter or emitter arrays at infrared and visible wavelengths. The high brightness exhibited by the diode-laser source can only be transferred to the application area by a very high-quality collimation of the emitted radiation. This starts at the very first lens after the laser facet, where the highest numerical aperture of the optical imaging system is needed.

Especially for applications with an array of several diode laser emitters on a single substrate along a common emission facet (known as "bar"), a cylindrical collimation system common to all emitters proves most useful

An optical imaging system of highest quality is needed for single-mode lasers and arrays thereof. Future application fields for fast axis aspheric laser collimators include the use of the diode laser in integrated external cavity systems for wave-length and mode stabilisation.

***Figure 1**: Plane aspheric fast axis collimators with different focal length*

Optical design considerations

High-power diode lasers are built from edge-emitting Fabry-Perot cavities on p-n-junctions in semiconductor crystals. The edge-emitting facets are formed by cleaving resonator mirrors along crystal lattice surfaces and coating them. The lateral dimensions of the laser cavity are determined by the epitaxial processing of the base wafer material. The wave-guiding properties of the laser cavity provide varying resonator functions such as single mode emitter, broad area emitter or amplification by trapezoid geometry.

All of these laser-cavities are also available in parallel structures aligned at a defined pitch in an array on a common semiconductor substrate known as a diode laser bar. They have an almost single mode Gaussian laser emission in the axis vertical to the p-n interface, commonly known as the fast axis (fast rate of increase of spot-size in free-space due to the larger divergence) and different degrees of mode content in the horizontal axis along the p-n interface known as slow axis.

Optical design considerations

The very high quality of the diode laser emission in the fast axis is advantageous in different coupling and application schemes. Collimation and imaging with rotationally symmetric optics is useful only when the spot-size ellipticity or the prevailing astigmatism is not of any importance to the application, or when enough space is available for subsequent anamorphotic magnification or correction. Cylindrical collimation and imaging optics, however, offer the advantage of simultaneous anamorphotic magnification and correction for astigmatism of the diode laser.

Due to the very small aperture of the diode laser waveguide along the fast axis, collimation in this direction usually is achieved with cylindrical lenses with a numerical aperture (NA) of the order of NA>0.8. Optical solutions looked into for this purpose are numerous. They range from spherical plano-convex lens systems with various high refractive indexes, over combined systems made from different plano-convex cylinders to hybrid lens systems with diffractive or refractive aspheric correction layers, aspheric plano-convex lenses or spherical or plano-parallel graded index lenses.

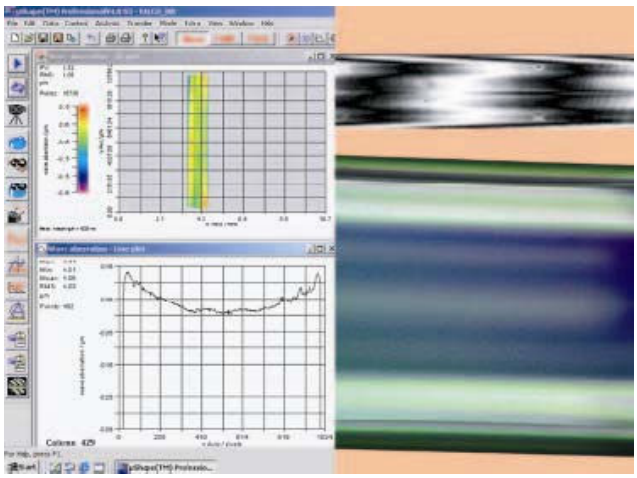

Figure 2: *Interferometric measurement of cylindrical FAC with FISBA's mPhase® 2 and mShape™ measurement and analysis software*

Process and Performance Parameters

The performance of the different optical systems can be theoretically compared in terms of the residual wave-front distortion (See figure 2).
Each has specific advantages for certain applications. Nevertheless, under the aspect of optimum quality and the concurrent demand for economic production processes, the optical design of the aspheric plane convex system is the most performing and is therefore used for collimation and imaging purposes in various applications.
The aspheric design parameters used for the second surface of the plano-convex system depend on the desired focal length. However, for actual systems the aspheric constants up to the third order are by far sufficient to reach the diffraction limit.
The main drawback with the cylindrical collimation systems is found in the imperfect optical performance with respect to the oblique rays emitted in directions between fast and slow axis.

Most important for high brightness applications is an optimum surface quality and an effective broadband anti-reflection coating. For specific applications targeting only one wavelength the coating can even be optimised to reach values of less than 0.1% residual reflection loss per surface.
The focal length can be produced in a range from as low as 0.1 mm to 2.5 mm with NA>0.8. In this range, each focal length requires a specific aspheric design.
The production technologies available for the qualified production range from etching, grinding and polishing or wafer-scale fabrication together with appropriate coating and miniaturisation processes.

Optical Materials

The materials used for the fabrication of the aspheric fast axis collimators are chosen from the available high index glass types with a focus on glass with a low dispersion coefficient, when the lenses are to be applied with diode lasers at a spectral range in the near IR-band. Before being processed the glass is checked for the homogeneity of the refractive index. Only very high index materials (n>2.3) are able to minimise the spherical aberration to acceptable values, when focusing with spherical fast axis collimators.

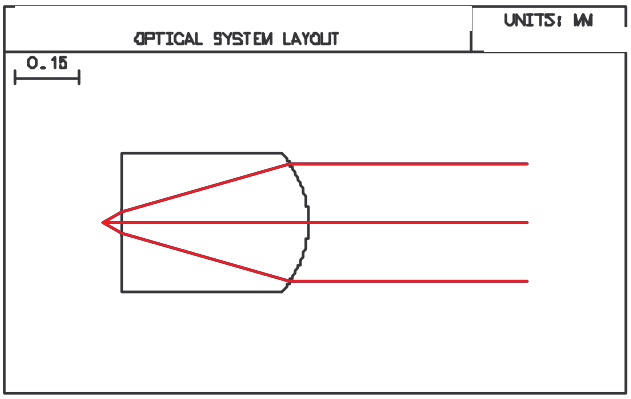

Figure 3a: *Optical design layout for a plane-aspheric FAC with f = 300 microns*

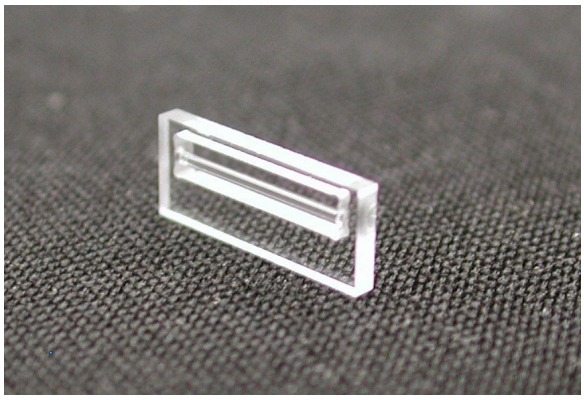

Figure 3b: *Mechanical design layout for a FAC with f = 300 microns and FAC-mount (width of the holder 12 mm)*

Typical manufacturing tolerances

Special factors affect the relation between the effective focal length and the back focal length which is the distance between the laser facet and the first optical surface. The back focal length should be as small as possible. Assembly, however, requires a security margin of some 30-100 microns. Straightness tolerances of the optical focus line set special manufacturing demands in the different directions of the laser emission in fast axis as well as in beam direction.

It is most important, finally, that the active surfaces be kept absolutely free of any absorbing residuals leading to thermal heat-up and eventually to the destruction of the lens. A typical list of lens manufacturing tolerances is given in table 1.

The handling of micro-optic cylindrical lenses is critical for collimators with a focal length below approximately 0.5 mm. This is typically solved with specific mounts and assembly structures also used for joining the lenses with the diode lasers (Figure 3b for details).

	Value	*Typical tolerance*	*Unit*	*Remark*
Effective focal length	0.1 -2.5	0.005 – 0.05	mm	EFL
Residual divergence	< 1.5	0.1	mrad	@ EFL = 1.0 mm
Numerical Aperture	>0.8	0.05		NA
Anti-Reflection Coating	> 98%	0.005%		780- 1000 nm
Transmission				
Back focal length	0.01-0.15	0.05	mm	

Table 1: *Typical manufacturing tolerances for plano-aspheric cylindrical laser collimator*

Interferometric quality control

To verify the performance, the lenses can be measured interferometrically with the FISBA's mPhase® 2 Twyman-Green digital interferometer. The mega-pixel resolution of this CCD-based evaluation allows for full qualification along the cylindrical axis in a single interferometric measurement (see figure 2)
Additional direct testing concerns the optical performance in cooperation with diode laser emission. In these tests, either the residual power in the imaged pedestals or the transmission through variable slit widths is utilised for a qualification of the performance (See figure 4).

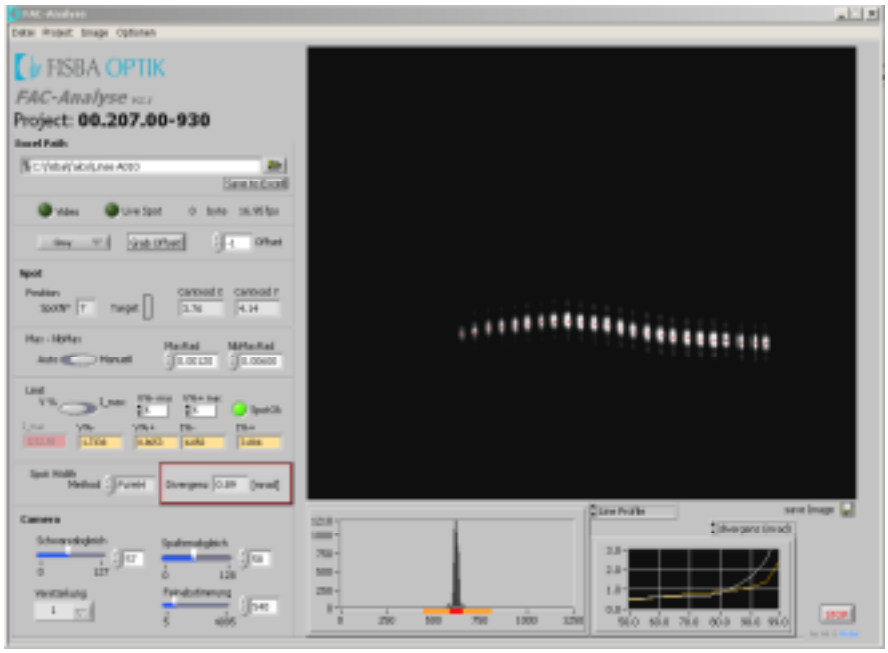

***Figure 4**: FAC performance evaluation in imaging mode with a high-power diode laser. The imaging is realised with an anamorphotic system imaging each individual emitter of a diode array in collimation position of the FAC. The grey scale image is evaluated for the vertical distortion of the combined FAC and diode laser (SMILE) as well as for the individual imaging quality of every emitter. The lower graph insert shows the vertical intensity distribution of a single emitter*

Comments and Outlook

The future driver of the FAC-performance is the availability of low cost and optimised standard designs for specific industrial applications. The residual wave-front distortion as well as the transmission properties still can be optimised. Further development trends are given with the requirement for shorter focal length as well as the integration of specific and optimised assembly structures, which will allow for processes adapted to low cost industrial assembly of micro-optic components and high-power diode lasers.

References

R. Diehl, U. Brauch, High Power Lasers for Direct Applications, in "High Power Lasers" ; Springer Verlag, IBSN: 3-540-66693-1

Quantum Dot Material for Uncooled High Brightness Laser Diodes

S. Deubert[1], W.Kaiser[1], J.P. Reithmaier[2] and A. Forchel[1]

[1]*Technische Physik, Universität Würzburg, Am Hubland, D-97074 Würzburg, Germany*

[2]*present address: Institut für Mikrostrukturtechnologie und Analytik, Technische Physik, Universität Kassel, Heinrich-Plett-Str. 40, D-34132 Kassel, Germany*

Introduction

Since the first realization of semiconductor lasers about 40 years ago, tremendous improvements in device performance have been achieved. The technology of the device fabrication was advanced at an enormous rate and intensive research and development provided a deeper insight in the underlying physical effects. But only the implementation of quantum wells in the carrier recombination zone, which was first realized in the end of the 70s of the last century [1], made the breakthrough of semiconductor lasers possible. The reduction of the dimension of the active region leads to a discretization of the energy states due to quantum mechanical principles. As a consequence, a strongly reduced threshold current density as well as an increased material gain is permitted [2].

Nevertheless, many theoretical studies were conducted in order to allow a further enhancement of semiconductor devices. At the beginning of the 80s of 20th century, Arakawa and Sakaki pointed out that a further reduction of the dimension of the active region could improve the device performance of semiconductor lasers [3]. Due to the carrier confinement in all three dimensions, quantum dots should exhibit a significantly reduced threshold current density and an enhanced temperature stability [4]. However, it took more than a decade to progress from the theoretical prediction to the first realization of quantum dot (QD) lasers. Only since 1994, has the material quality and the fabrication technique of quantum dots been good enough to allow the first laser with a quasi zero-dimensional gain region [5]. Due to further improvements, QD lasers nowadays already show device properties comparable to high performance QW structures [6], while some features are even superior.

Owing to the three-dimensional carrier confinement, quantum dots show a discrete energy spectrum with splitting energies controlled by the geometric size. This discretization of the energy spectrum results in a δ-peak as density of states and therefore to a density of states at the laser energies, which is much higher than in bulk or quantum well materials, so that a strongly improved probability of stimulated emission in laser structures is obtained. As a result a higher spectral gain as well as a reduced threshold current density can be achieved with quantum dot devices. The newest publications show that lasers with quantum dots as the active region exhibit ultra-low threshold current densities with record values of only 17 A/cm^2 [7]. In addition, further important effects make quantum dots especially attractive for semiconductor laser applications. So it is possible to tailor specific material properties by the dot geometry itself. As the quantum dots provide lower energy states than the surrounding quantum well material, the recombination occurs spatially localized at the dot positions. This localization results in a reduced carrier diffusion length and therefore a reduction of the leakage current is expected. Additionally, the symmetric gain profile of quasi zero-dimensional active regions leads to a small α-factor [8], which has a great influence on many important device effects. A low α-factor improves the high frequency properties (chirp) and leads to a reduced filamentation, which is of special interest for high brightness applications.

To analyze the dependency of the beam profile on the dimension of the active region, different high brightness lasers were fabricated in cooperation with Thales Research and Technology. Tapered lasers based on quantum dot and quantum well material were realized and the near-field pattern was measured at various output powers. Especially at a higher output power above 1 W, the quantum dot device shows a noticeable reduction of the filamentation, which correlates with the smaller linewidth enhancement factor α [9]. In Fig. 1, the near-field patterns of two identical tapered lasers with different active regions are depicted at an output power of 2 W. But only the QD device shows a Gaussian beam profile, which demonstrates the advantages of quantum dots as the active region in high brightness devices.

Growth of Self-Assembled Quantum Dots

The realization of the application relevant quantum dots became possible by the introduction of self-organized growth based on metal organic vapor phase epitaxy (MOVPE) and molecular beam epitaxy (MBE). These techniques are capable of the controlled deposition of a fraction of an atomic monolayer and exhibit an enhanced dot quality compared to prior etching or overgrowth methods. The driving force behind the self-formation is the lattice mismatch between the underlying semiconductor layer and the dot material. In the case of lasers emitting in the 1 µm wavelength region, dots realized by $In_{0.6}Ga_{0.4}As$ on GaAs barriers showed the best results. The lattice mismatch leads to self-assembled quantum dots with a high dot density of about 1×10^{11} cm^{-2} and a good homogeneity with small size fluctuations. Thus, the gain is very high and a single quantum dot layer is sufficient to drive a laser device. Various layer designs were already studied to establish quantum dots for different laser applications at various emission wavelengths. Today, GaAs-based quantum dot lasers emitting in the wavelength range between 900 nm and 1.3 µm are main part of the research of various working groups. Due to the simplicity of the self-formation, the principle of self-assembly can easily be transferred to different material compositions [10-12], so that a wide wavelength range can be covered easily.

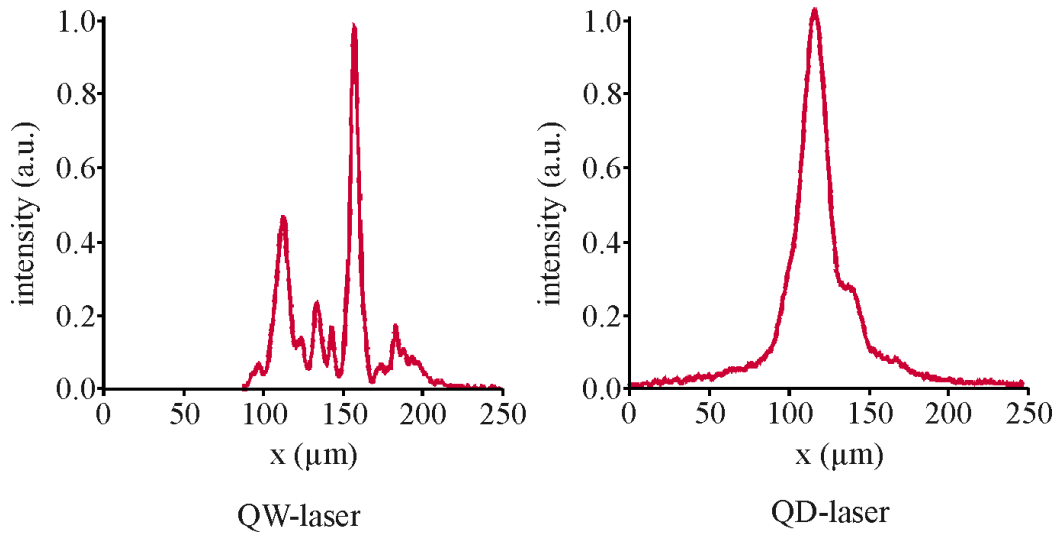

Fig. 1: Near-field patterns of tapered lasers diodes at an output power of 2 W. The QD laser shows a clearly reduced filamentation compared to the quantum well reference (measured by Thales R&T) [13].

Temperature Stability

Especially for fiber amplifier modules, high power pump sources with a temperature stable device performance are of special interest. Because the temperature stabilization is expensive and power consumptive, lasers with a reduced thermal induced wavelength shift are preferred. With QD lasers, the temperature stability of the emission wavelength can be enhanced significantly without deteriorating the basic device performance. By a specific design of the quantum dot geometry in combination with an appropriate waveguide structure and an optimized optical confinement factor, the temperature dependence of the emission wavelength can be reduced by a factor of more than three in comparison to conventional QW lasers. In Fig. 2, the thermal induced wavelength shift of different laser designs is depicted. 100 µm wide broad area lasers with emission wavelengths in the range of 1 µm were measured under pulsed excitation with a duty cycle of 0.03 % at different temperatures between 20 and 80 °C. According to Eq. 1, an increase of the operation temperature leads to reduction of the band gap energy.

$$E_g(T) = E_0 - \frac{\alpha \cdot T^2}{T + \beta} \qquad (1)$$

With temperature independent material parameters E_0, α and β.

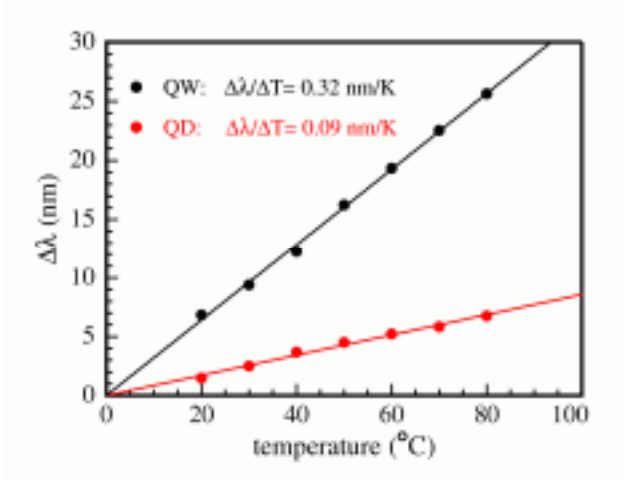

Fig. 2: Thermal induced shift of the emission wavelength as a function of the operation temperature.

This shrinking of the band gap results generally in a red shift of the emission. Therefore, the quantum well laser shows a thermally induced wavelength shift of 0.32 nm/K, which is typical for GaInAs QW lasers in this wavelength range. With quantum dot active regions, this behavior can be improved significantly. Owing to their flat gain profile, QD lasers can partially compensate the inevitable red shift of the wavelength [14], which results in a more stable emission wavelength. To illustrate this effect, the spectral gain functions for different carrier densities are plotted in Fig. 3. For the QD structure, the ground and first excited transition state are taken into account and a Gaussian shape broadening is assumed.

In semiconductor lasers, an increase in temperature generally leads to higher internal absorption and therefore higher carrier intensities are needed to achieve lasing. But with increasing carrier densities, the gain maximum shifts towards higher energy due to the increased state filling. While the energy shift is relatively small in QW lasers, QD lasers exhibit a much larger blue shift of the gain maximum. This blue shift can partially compensate the aforementioned red shift, which is caused by the shrinking band gap. Especially near the flat region of the gain curve of the QD lasers, an increase in carrier density leads to a large energy shift and therefore to a temperature stable emission wavelength. By tailoring the dot geometry, the slope of the gain curve can be improved, which results in an optimized thermal stability with wavelength shifts as low as the temperature-induced change of the refractive index [15]. Quantum dot samples with a larger energy splitting between the ground and first excited transition states exhibit a very flat gain profile and thus a wavelength shift of less than 0.1 nm/K [13]. Similar effects can be seen with InP or GaSb based QD lasers emitting in different wavelength regions [16, 17], which confirms the unique quantum dot feature.

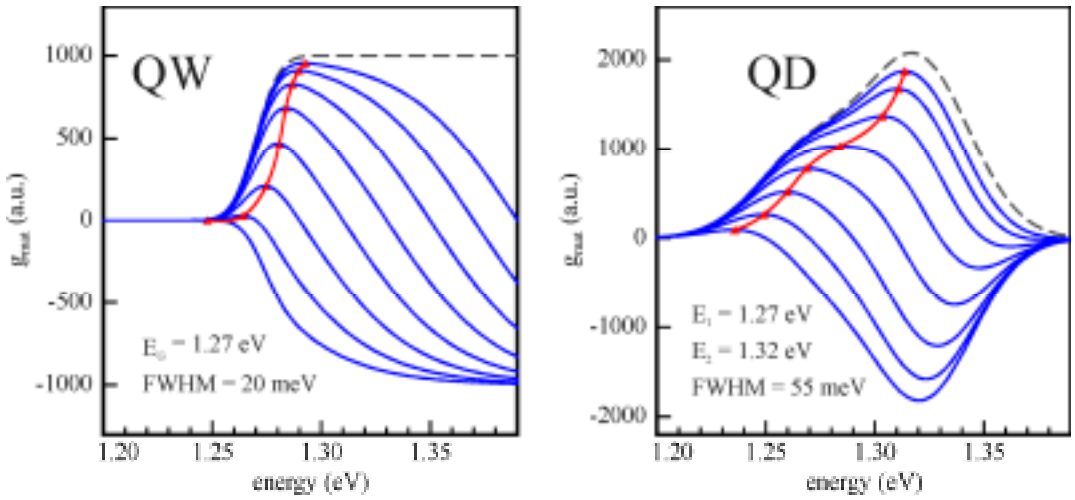

Fig. 3: Theoretical material gain for different quasi-Fermi levels in case of a quantum well (QW) and a quantum dot (QD) active region.

High Power Device Performance

High power diode lasers using a quantum well as active region are state-of-the-art and output powers up to 16 W from a 100 µm wide facet were already published [18]. But due to the small linewidth enhancement factor and the aforementioned very good temperature stability and reduced filamentation, quantum dot lasers are a promising alternative to conventional devices. In Fig. 4, the light output characteristic of a 100 µm wide and 1 mm long broad area quantum dot laser is depicted. The measurement was performed under continuous wave conditions at 12 °C. Despite the improved temperature stability, this laser exhibits a high output power of more than 3 W at a drive current of 3.5 A.

A high slope efficiency emphasizes the good device properties and results in a high wallplug efficiency of 55 % at an injection current of 1.7 A. Similar results were already obtained with QD lasers at various emission wavelengths [19, 20] and 100 µm wide lasers with quantum dots as the gain region have already shown output powers up to 6.3 W [21].

Temperature dependent measurements reveal a good thermal stability of the basic device data, so that even at an operation temperature of 100 °C, a total output power of more than 1 W could be obtained. These device data are comparable to high performance QW lasers and prove the suitability of quantum dot lasers for the realization of uncooled high power pump modules.

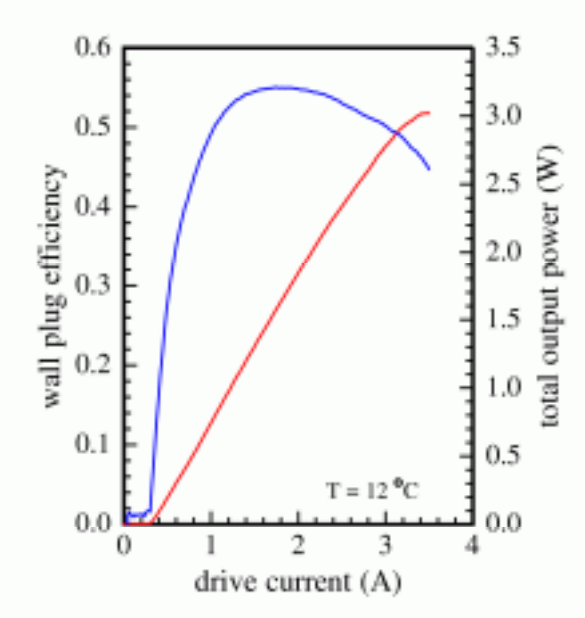

Fig. 4: CW light output characteristic of a 1 mm long and 100 µm wide broad area quantum dot laser at 12 °C.

Summary

Since the first realization of semiconductor quantum dot lasers, much progress has been made to improve the device performance. Owing to the three-dimensional carrier confinement, quantum dots show various advantages that render them superior to conventional quantum well lasers like the unique possibility to tailor the material properties directly by the quantum dot geometry. Reduced threshold current densities together with a small α-factor make QD material advantageous for high brightness applications. Due to their flat gain profile, quantum dot devices have additionally an enhanced temperature stability of the emission with wavelength shifts less than 0.1 nm/K, which is nearly as low as the change of the refractive index. Nevertheless, high output powers of more than 3 W and high wallplug efficiencies up to 55 % can be obtained, which proves the suitability of QD material for high power devices and demonstrates that quantum dot lasers are a possible solution for highly efficient, wavelength stabilized, uncooled high power pump modules.

References

[1] J.P. van der Ziel, R. Dingle, R.C. Miller, W. Wiegmann, and W.A. Nordland Jr.: 'Laser oscillation from quantum states in very thin GaAs-Al0.2Ga0.8As multilayer structures', *Appl. Phys. Lett.* ***26(8)****, pp. 463-465, (1975)*

[2] N. Holonyak, R.M. Kolbas, R.D. Dupuis, and P.D. Dapkus: 'Quantum-Well Heterostructure Lasers', *IEEE J. Quantum Electron.* ***16(2)****, pp. 170-186, (1980)*

[3] Y. Arakawa and H. Sakaki: 'Multidimensional quantum well laser and temperature dependence of its threshold current', *Appl. Phys. Lett.* ***40(11),*** *pp. 939-941, (1982)*

[4] M. Asada, Y. Miyamoto, and Y. Suematsu: 'Gain and the Threshold of Three-Dimensional Quantum-Box Lasers', *IEEE J. Quantum Electron.* ***22(9)****, pp. 1915-1921, (1986)*

[5] N. Kirstaedter, N.N. Ledentsov, M. Grundmann, D. Bimberg, V.M. Ustinov, S.S. Ruvimov, M.V. Maximov, P.S. Kop'ev, Zh.I. Alferov, U. Richter, P. Werner, U. Gösele, J. Heydenreich: 'Low threshold, large T0 injection laser emission from (InGa)As quantum dots', *Electron. Lett.* ***30(17)****, pp. 1416-1417, (1994)*

[6] F. Klopf, J.P. Reithmaier, and A. Forchel: 'Highly efficient GaInAs/(Al)GaAs quantum-dot lasers based on single active layer versus 980 nm high-power quantum-well lasers', *Appl. Phys. Lett.* ***77(10)****, pp. 1419-1421, (2000)*

[7] I.R. Sellers, H.Y. Liu, K.M. Groom, D.T. Childs, D. Robbins, T.J. Badcock, M. Hopkinson, D.J. Mowbray, and M.S. Skolnick: '1.3 μm InAs/GaAs multilayer quantum-dot laser with extremely low room-temperature threshold current density', *Electron. Lett.* ***40(22)****, pp. 1412-1413, (2004)*

[8] T.C. Newell, D.J. Bossert, A. Stintz, B. Fuchs, K.J. Malloy, and L.F. Lester: 'Gain and Linewidth Enhancement Factor in InAs Quantum-Dot Laser Diodes', *IEEE Photon. Technol. Lett.* ***11(12)****, pp. 1527-1529, (1999)*

[9] J.R. Marciante and G.P. Agrawal: 'Nonlinear Mechanisms of Filamentation in Broad-Area Semiconductor Lasers', *IEEE J. Quantum Electron.* ***32(4)****, pp. 590-596, (1996)*

[10] B. Junno, T. Junno, M.S. Miller, and L. Samuelson: 'A reflection high-energy electron diffraction and atomic force microscopy study of the chemical beam epitaxial growth of InAs and InP islands on (001) GaP', *Appl. Phys. Lett.* ***72(8)****, pp. 954-956, (1998)*

[11] R. Schwertberger, D. Gold, J.P. Reithmaier, and A. Forchel: 'Long-Wavelength InP-Based Quantum-Dash Lasers', *IEEE Photon. Technol. Lett.* ***14(6)****, pp. 735-737, (2002)*

[12] Y. Arakawa: 'Progress in GaN-Based Quantum Dots for Optoelectronics Applications', *IEEE J. Sel. Top. Quantum Electron.* ***8(4)****, pp. 823-832, (2002)*

[13] S.C. Auzanneau, M. Calligaro, M. Krakowski, F. Klopf, S. Deubert, J.P. Reithmaier, A. Forchel : 'High brightness GaInAs/(Al)GaAs quantum-dot tapered lasers at 980 nm with high wavelength stability', *Appl. Phys. Lett.* ***84(13)****, pp. 2238-2240, (2004)*

[14] F. Klopf, S. Deubert, J.P. Reithmaier, and A. Forchel: 'Correlation between the gain profile and the temperature-induced shift in wavelength of quantum-dot lasers', *Appl. Phys. Lett.* ***81(2)****, pp. 217-219, (2002)*

[15] S. Deubert, R. Debusmann, J.P. Reithmaier, and A. Forchel: 'High-power quantum dot lasers with improved temperature stability of emission wavelength for uncooled pump sources', *Electron. Lett.* ***41(20)****, pp. 1125-1127, (2005)*

[16] J.P. Reithmaier and A. Forchel: 'Recent advances in semiconductor quantum dot lasers', C. R. Physique ***4****, pp. 611-619, (2003)*

[17] Y. Qiu, D. Uhl, and S. Keo: 'Room-temperature continuous-wave operation of InAsSb quantum-dot lasers near 2 µm based on (001) InP substrate', Appl. Phys. Lett. ***84(2)****, pp. 263-265, (2004)*

[18] N.A. Pikhtin, S.O. Slipchenko, Z.N. Sokolova, A.L. Stankevich, D.A. Vinokurov, I.S. Tarasov, Z.I. Alferov; '16W continuous-wave output power from 100 µm-aperture laser with quantum well asymmetric heterostructure'*, Electron. Lett.* ***40(22)****, pp. 1413-1414, (2004)*

[19] A.R. Kovsh, A.E. Zhukov, D.A. Livshits, A.Yu. Egorov, V.M. Ustinov, M.V. Maximov, Yu.G. Musikhin, N.N. Ledentsov, P.S. Kop'ev, Zh.I. Alferov, and D. Bimberg: '3.5W CW operation of quantum dot laser'*, Electron. Lett.* ***35(14)****, pp. 1161-1163, (1999)*

[20] A.Wilk, A.R. Kovsh, S.S. Mikhrin, C. Chaix, I.I. Novikov, M.V. Maximov, Yu.M. Shernyakov, V.M. Ustinov, N.N. Ledentsov: 'High-power 1.3 µm InAs/GaInAs/GaAs QD lasers grown in a multiwafer MBE production system'*, J. Cryst. Growth* ***278****, pp. 335-341, (2005)*

[21] B. Sumpf, S. Deubert, G. Erbert, J. Fricke, J.P. Reithmaier, A. Forchel, R. Staske, and G. Tränkle: 'High-power 980 nm quantum dot broad area lasers'*, Electron. Lett.* ***39(23)****, pp. 1655-1657, (2003)*

Operating Principles and Performance Limits of High Brightness Tapered Lasers

I. Esquivias[1], H. Odriozola[1], J.M. García Tijero[1], L. Borruel[1], S. Sujecki[2], and E. C. Larkins[2]

[1]*ETSI Telecomunicación, Univ. Politécnica de Madrid, Ciudad Universitaria s/n, Madrid 28040, Spain*

[2]*School of Electrical and Electronic Engineering, University of Nottingham, Nottingham NG7 2RD, UK*

1. Introduction

The Brightness of an optical source is defined as the power per unit emitting area and per unit solid angle into which the power is emitted [1]. The Brightness depends on the emitted power and on the beam quality, which is usually measured by means of the "beam parameter product", the product of the minimum diameter of the beam and its divergence. The most usual figure of merit for the beam quality is the M^2 coefficient, which is the beam parameter product normalized to that of an ideal Gaussian mode. A value $M^2 = 1$ represents an ideal diffraction limited source, while values higher than unity indicate a degradation of the beam quality.

Semiconductor lasers are optical sources with very well known advantages over other types of optical sources: small size, high conversion efficiency and low cost. Many applications of semiconductor lasers demand high brightness, such as material processing, optical pumping of solid state and fiber lasers, medical treatments, optical wireless communications, and all applications generally requiring high power launched into an optical fiber. However, the brightness of a semiconductor laser is usually limited due to the contradictory requirements needed to achieve high brightness: a large emitting area is required to produce high power with reduced bulk and surface heating, while reduced dimensions are required to maintain a single spatial mode and its correspondingly high beam quality. High power semiconductor lasers are based on broad area (BA) devices, with a poor beam quality along the slow (lateral) axis, while devices with reduced lateral dimensions and good beam quality, such as ridge waveguide (RW) lasers, suffer from a limited maximum output power.

In consequence, an important research effort during the last years has been devoted to improve the brightness of semiconductor lasers. Various new approaches have been proposed, including lasers with a tapered gain region, the master-oscillator power amplifier configuration, and the angled grating distributed feedback laser (see [1-2] and references herein for details and description of other approaches). Tapered lasers, also called flared unstable cavity lasers [1-20], are possibly the best choice to achieve high brightness at moderate cost, due to the technological simplicity of their fabrication process. In fact, a relatively high number of industrial and research laboratories are presently developing tapered lasers, and, as far as we know, they are presently the only type of high brightness semiconductor laser commercially available.

The first technical paper on the operation of a tapered laser was published in 1993 by the group at the Massachusetts Institute of Technology led by J.N. Walpole [3]. These devices operated at 980 nm and achieved an output power of 4.2W with good beam quality. Since then, tapered lasers at different wavelengths and with different designs have been reported [3-20]. Tables I and II summarize the best reported performances to date for single emitter tapered lasers, and for arrays or bars based on tapered lasers, respectively.

λ(µm)	Material	Max. Power	M² (@ Power)	Geometry IG/GG	L_{tot}	angle	Year, Ref.
0.642	AlInGaP	0.9 W cw	$M^2 \leq 3$ (@ 0.7 W)	GG			2004 [4]
0.735	GaAsP/AlGaAs	3.3 W	$M^2(1/e^2) < 1.5$ (@ 1.5 W)	GG,	2.75 mm,	6º	2003 [5]
0.808	GaAsP/AlGaAs	5.0 W cw	$M^2(1/e^2) = 1.3$ (@ 3.9 W)	GG,	2.75 mm,	6º	2006 [6]
0.915	AlGaInP/GaInP/GaInAs	1 W cw	$M^2(1/e^2) = 3$	IG,	2.5 mm,	<1º	2005 [7]
0.915	AlGaInP/GaInP/GaInAs	0.65 W cw	$M^2(1/e^2) = 1.3$	IG,	2.5 mm,	2º	2005 [7]
0.94	InGaAs/AlGaAs	5.3 W cw	$M^2(1/e^2) < 1.3$ (@ 2.2 W)	GG,	3 mm,	6º	2002 [8]
0.98	InGaAs/AlGaAs	12.5 W cw	$M^2(1/e^2) = 1.4$ (@ 8.3 W)	GG,	3.5 mm,	6º	2005 [9]
0.98	InGaAs/AlGaAs	1.1 W cw		IG,	2.5 mm,	<1º	2005 [10]
0.98	InGaAs/GaAsP/AlGaAs	5.5 W cw	$M^2(1/e^2) < 1.5$ (@ 5.3 W)	GG,	4 mm,	6º	2005 [11]
1.04	InGaAs/AlGaAs	4.0 W cw	$M^2(1/e^2) = 1.4$ (@ 4 W)	GG,	2.5 mm,	6º	2003 [12]
1.3	InGaAsP/In	1 W cw			3mm		1996 [13]
1.47	InGaAsP/InP	1.6 W cw	$M^2(1/e^2) < 1.4$ (@ 1 W)	GG,	2.5 mm,	6º	2005 [14]
1.48	InGaAsP/InP	1.75 W cw		GG,	2.3 mm,	6º	2001 [15]
1.91	GaInSb/AlGaAsSb	0.9 W cw	$M^2 \leq 1.7$ (@ 650 mW)		2.5 mm		2005 [16]

Table I: Best reported performance of single emitter tapered lasers

λ(µm)	Material	Max. Power	M²	Geometry IG/GG	L_{tot}	angle	Bar width	Year, Ref.
0.98	InGaAs/InGaAsP	20 W cw		IG,	2.5 mm,	<1º,	3 mm	2003 [17]
0.98	InGaAs/AlGaAs	25 W cw	2.6		2 mm,	6º,	10 mm	1999 [18]
0.98	InGaAs/AlGaAs	9.5 W cw			2 mm,	0.95º,	0.33 mm	1999 [19]
1.59	InGaAs/InP	1.4 W cw		IG,	1 mm,	2.15º,	0.33 mm	1998 [20]

Table II: Best reported performance of laser bars or arrays based on tapered lasers.

The maximum achievable brightness in tapered lasers is not limited by thermal effects or by catastrophic optical damage (COD) as in BA devices, but by beam deterioration due to non-linear effects, such as self-focusing and filamentation [21-22]. A clear understanding of the mechanisms limiting the device performance is of great interest in order to propose and fabricate new designs with improved brightness. Numerical simulations, properly validated by comparisons with experimental results, are a valuable tool for improving our physical insight into the non-linear interactions between optical, electrical and thermal phenomena inside the unstable resonator, as well to provide optimized designs with minimum experimental effort.

The groups at the University of Nottingham and at the Universidad Politécnica of Madrid, partners of project WWW.BRIGHT.EU, have developed a sophisticated simulator for tapered lasers, called CONAN, which solves the electrical, optical and thermal equations for these devices (see [21, 22] for a detailed description of the model). Despite the assumptions needed to reduce the model complexity (steady state, single frequency, two-dimensional propagation of the optical mode), the simulations have shown good qualitative and quantitative agreement with experimental results in tapered lasers with different geometries and based on different materials [21, 22]. Furthermore, the simulator has demonstrated to be a useful tool to predict the behaviour of novel designs prior to their fabrication [23]. Other models in literature [24, 25], based on similar approaches, have also reproduced the main trends observed experimentally.

In this article, we present a comprehensive description of the operating principles and limitations of high brightness tapered lasers. The description is based on the simulations of real devices fabricated by Alcatel-Thales III-V Labs [7, 17] and by Ferdinand-Braun-Institut für Höchstfrequenztechnik [2, 5]. In section 2, the usual device geometry and the operating principles of the tapered laser are presented by analyzing the beam propagation inside the cavity of typical devices. In section 3, the physical origin of the limitations in the maximum brightness is described.

2. Device geometry and basic operating principles

Tapered lasers consist of two coupled sections (see Fig. 1): a ridge waveguide (RW) section, and an index or gain guided tapered section. The RW section provides a single spatial mode which is launched into the tapered section, where it is amplified while preserving its shape.

The length of the RW section L_{RW} is typically around 500 µm, although values ranging between 200 µm [19] and 1000 µm [2] have been reported. The total cavity length L_T was 2 mm in initial designs [19], with a trend towards longer cavities, up to 4 mm, in recent years [11]. Two clearly different types of tapered sections have been reported to date: gain guided (GG) tapers with a relatively large full taper angle θ_{tap} (typically 4-8º, depending on wavelength), designed to match the free diffraction angle as we will describe later [2-6, 8-9, 11-12, 14-15, 18], and narrow index guided (IG) tapers with small angle (<1º) [7, 10, 17, 20].

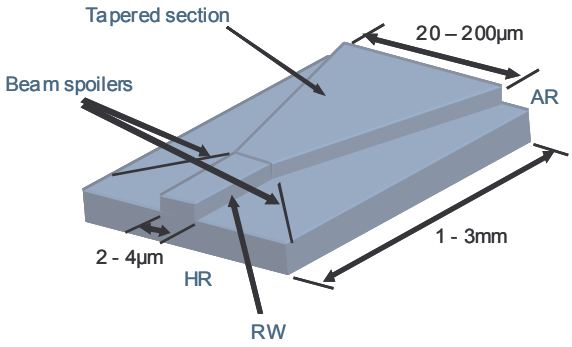

Fig. 1: Schematics of a typical tapered laser

The laser facets are coated to achieve high reflectance (HR) at the back facet of the RW, typically around 95%. Similarly, the front facet of the tapered section receives a low reflectance (anti-reflective, AR) coating, with values ranging between 0.1% and 3%. In most of GG tapered laser designs, a spatial filter or beam spoiling aperture is formed by etching the region adjacent to the RW section, so that the portions of the beam associated with the excitation of higher order optical modes are scattered out of the device.

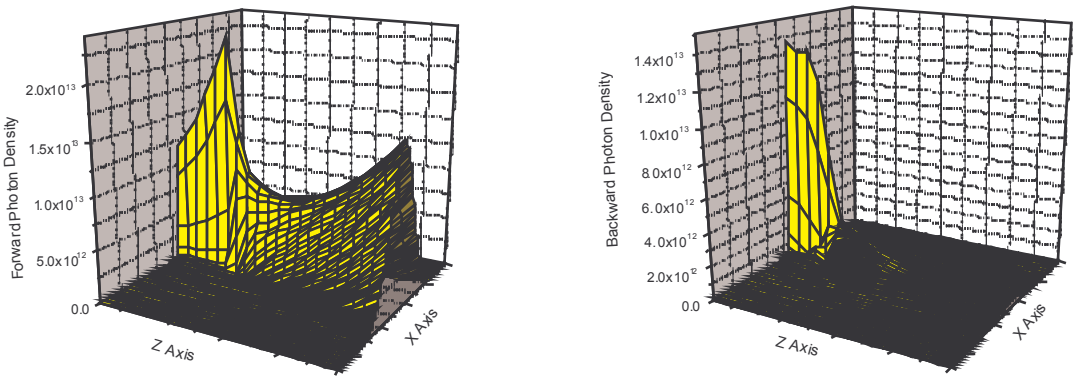

Fig. 2: Simulated forward (a) and backward (b) optical field intensity inside the cavity for the GG tapered laser described in the text, when operated at low power.

We analyze the basic operating principles of tapered lasers by considering as an example a typical device emitting at 980 nm: 500 µm long and 3 µm wide RW section, 1500 µm long GG tapered section with a full taper angle of 4º, yielding an output aperture of 107.7µm. Figs. 2a and 2b illustrate the shape of the forward and backward optical field intensities at low power (slightly above threshold) and under isothermal conditions. The shape of the fundamental mode of the RW section which is launched into the gain section (see curve A in Fig. 3a) can be approximated by a Gaussian function. The calculated full width of the mode at $1/e^2$ (W_{mode}) for this example, with an index step of $2.2 \cdot 10^{-3}$, is 5.2 µm.

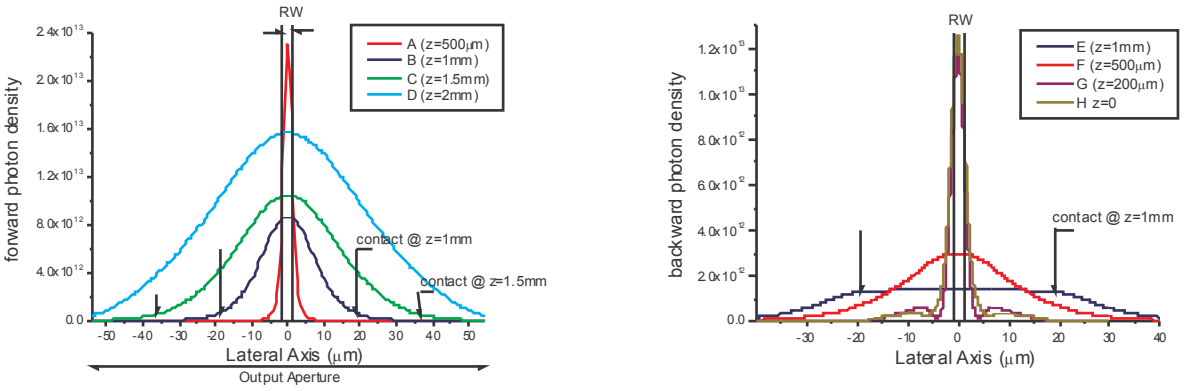

Fig. 3: Simulated forward (a) and backward (b) optical field intensities at different positions inside the cavity for the GG tapered laser, when operated at low power.

When entering into the tapered section, the mode is subject to two different effects: i) amplification by the gain medium; and ii) free diffraction if the full taper angle is larger than the free diffraction full angle θ_D (at $1/e^2$). The free diffraction angle of an ideal Gaussian beam is given by:

$$tg\left(\theta_D/2\right) = \frac{2 \cdot \lambda}{\pi \cdot n_{eff} \cdot w_{mode}} \qquad [1]$$

where n_{eff} is the effective index of the vertical waveguide and λ the emitting wavelength.

In the case of the example device under analysis, the full taper angle has been chosen to match the value of θ_D arising from expression [1], around 4º. Fig. 3a shows the intensity of the forward traveling light at cross-sections taken along the tapered region (z = 1 mm, curve B and z= 1.5 mm, curve C – note that z=0 is the back facet) and the intensity reaching the output facet (curve D). The intensity at the beam center is smaller than that of the launched mode (see Fig. 3a). The beam reaching the output facet has a Gaussian-like shape, although the wavefront has a convex shape, so that the phase at the facet is far from uniform. The reflected (or backward) intensity continues diffracting but now the gain medium does not overlap with the freely diffracting beam and the gain guiding reduces its width. Fig. 3b shows the intensity of the backward field at the center of the tapered section and at the entrance of the RW section (curves E and F, respectively). As the beam entering into the straight section is wider than the fundamental mode of the ridge waveguide (48.3 µm and 5.2 µm at $1/e^2$, respectively, in this example), a substantial part of the power is not coupled producing the so-called coupling losses [1] or taper losses [26]. The beam propagating along the RW section is filtered by the single-mode waveguide, with the help of the beam spoilers, if they exist in the design. The field intensities at the middle of the RW and at the back facet for our example, which includes a beam-spoiling aperture, are shown in curve G and H of Fig. 3b, respectively. The beam at the back facet is still slightly wider than the single-mode of the waveguide, and side lobes are still present, but it recovers the original shape during the way towards the tapered section and through a second filtering process by the beam spoilers.

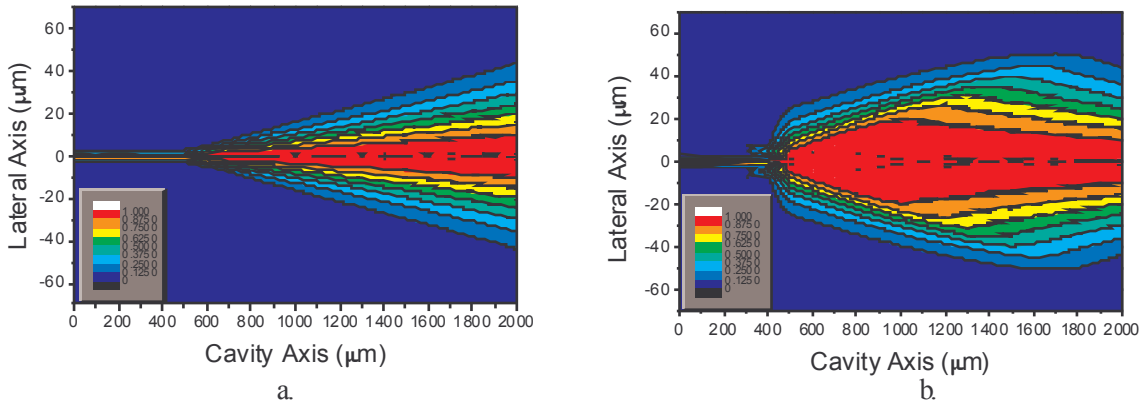

Fig. 4: Normalized forward (a) and backward (b) optical field intensity inside the cavity for the GG tapered laser, when operated at low power.

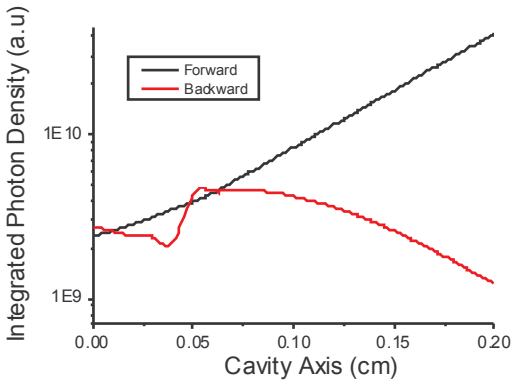

Fig 5: Integrated Photon density for the forward and backward traveling optical fields along the cavity for the GG tapered laser, when operated at low power.

The evolution of the shape of the beam inside the cavity can be visualized with the help of the color plot in Fig. 4, where the forward (Fig. 4a) and backward (Fig. 4b) photon densities have been normalized by the peak density at each longitudinal position. The evolution of the beam power along the cavity is shown in Fig. 5, where we have integrated the forward and backward photon densities in the lateral dimension at each longitudinal position. In the logarithmic scale of Fig. 5, an exponential power growth is represented by a straight line, as it happens in the tapered region for the forward beam. The backward beam shows initially an exponential growth in the tapered section due to the good overlap with the pumped region. The beam amplification decreases at the end of the tapered region, due to the reduced overlap with the gain region. After entering into the RW section, the total power decreases by the effect of the beam spoilers. A slight amplification is observed in the RW section, where filtering and gain are competing mechanisms decreasing and increasing the power, respectively.

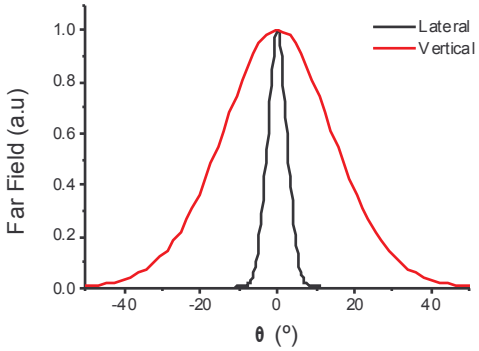

Fig. 6. Far Field intensities for the GG tapered laser, when operated at low power.

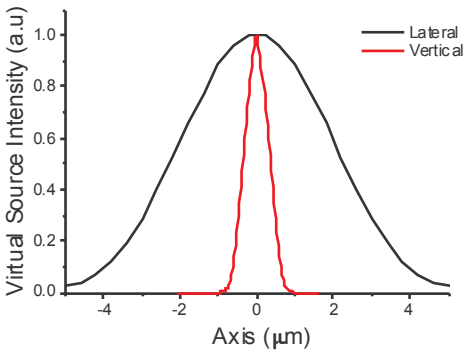

Fig. 7. Virtual source intensities for the GG tapered laser, when operated at low power.

The lateral far-field (FF) pattern for the device in this example is shown in Fig. 6, where the vertical FF is also shown for comparison. The angular width of the lateral FF can be estimated by applying Snell´s law to the beam at the output facet. In this case, this yields a full beam divergence angle θ_{out} (at $1/e^2$) ~ $n_{eff} \cdot \theta_D = 3.4 \cdot 4^o = 13.6^o$ (n_{eff} ~ 3.4). The simulations at low output power predict a value for θ_{out} of 10.3º, not far from the previous estimation. The beam is strongly astigmatic, as the virtual source (or beam waist) is located at the distance behind the front facet $z_{vs} = 0.5w_o/\sin(q_{out}/2) \sim 0.5w_o/(n_{eff} \sin(q_D/2))$. If $q_D = q_{tap}$, then $z_{VS} \sim L_{tap}/ n_{eff}$ where L_{tap} is the length of the tapered section. In our example the simulations predict z_{VS} = 438 μm, close to L_{tap}/ n_{eff} = 440 μm. The calculated virtual source intensity is shown in Fig. 7, where the vertical mode profile is also shown for comparison. The width of the virtual source at $1/e^2$, w_{VS} (7.5 μm in our example), in conjunction with θ_{out} is often used to provide an experimental estimation of the beam quality by means of the so-called beam quality factor M^2 at $1/e^2$ [27], using the expression:

$$M^2\left(1/e^2\right) = \frac{\pi}{4 \cdot \lambda} \cdot \theta_{out} \cdot W_{VS} \quad , \qquad [2]$$

which takes a value of 1.1 in our example, when operating close to threshold. A more correct characterization of the beam quality is given by the second moment M^2, which can be experimentally determined from the measured evolution of the beam radius along the propagation direction [28]. The calculated value in our example is also around unity, indicating that an optimal beam quality is obtained in tapered lasers at low power.

We analyze now the properties of an IG tapered laser with a narrow taper angle and illustrate important differences in comparison with large angle GG devices. The single-mode pattern launched by the RW section into the tapered section does not expand by free diffraction. Instead, the beam expands according to the shape of the lateral waveguide, as defined by the refractive index step. Fig. 8a illustrates the forward beam propagation for an IG example device with same RW section width, length and index step as in the previous example, and with full taper angle of 0.9º. The beam expands adiabatically, preserving its shape, with most of the power (98% @ z=1mm) inside the guided region. The propagation of the backward field includes a combination of competitive phenomena: diffraction, gain and index guiding, reflections at the waveguide interface. In many cases, it develops a multilobed shape (see Fig. 8b). The index guiding, as well as the relatively small taper angle, produces a beam entering into the RW which is narrower than that of the GG devices, reducing hence the taper losses. The RW section acts again as a spatial filter, and the beam recovers its original single-mode shape after a complete round trip.

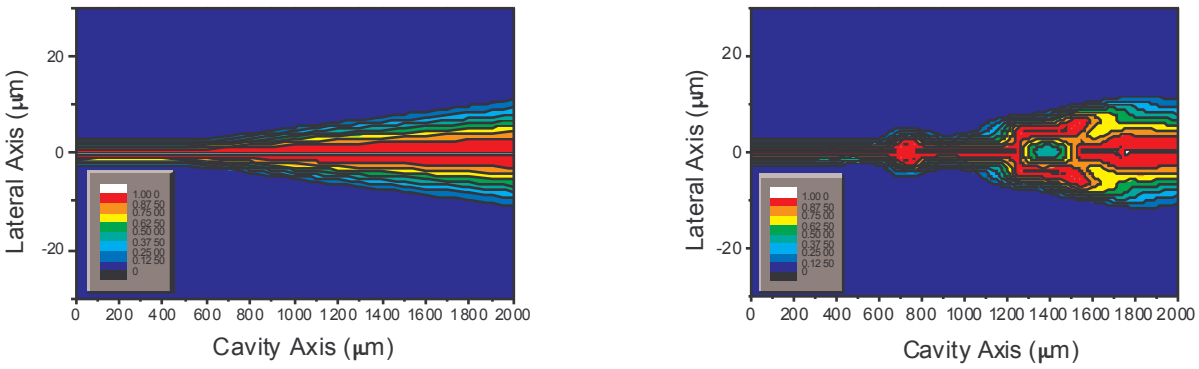

Fig. 8: Normalized forward (a) and backward (b) optical field intensity inside the cavity for the IG tapered laser described in the text, when operating at low power.

The output beam diffracts freely in the air, but now the angular width of the FF pattern is not so simply given by applying Snell´s law to the taper angle. It takes an intermediate value between that for free diffraction from the RW section and that for free diffraction from the output facet. In our example, the simulations predict $\theta_{out} = 4º$, while the free diffraction angle from the RW section, taking into account the change of medium would be 13.6º, as in previous example, and the free diffraction angle from the output aperture would be 2.7º. In consequence, the output beam also presents a non-negligible astigmatism at low power, 130 µm in our example.

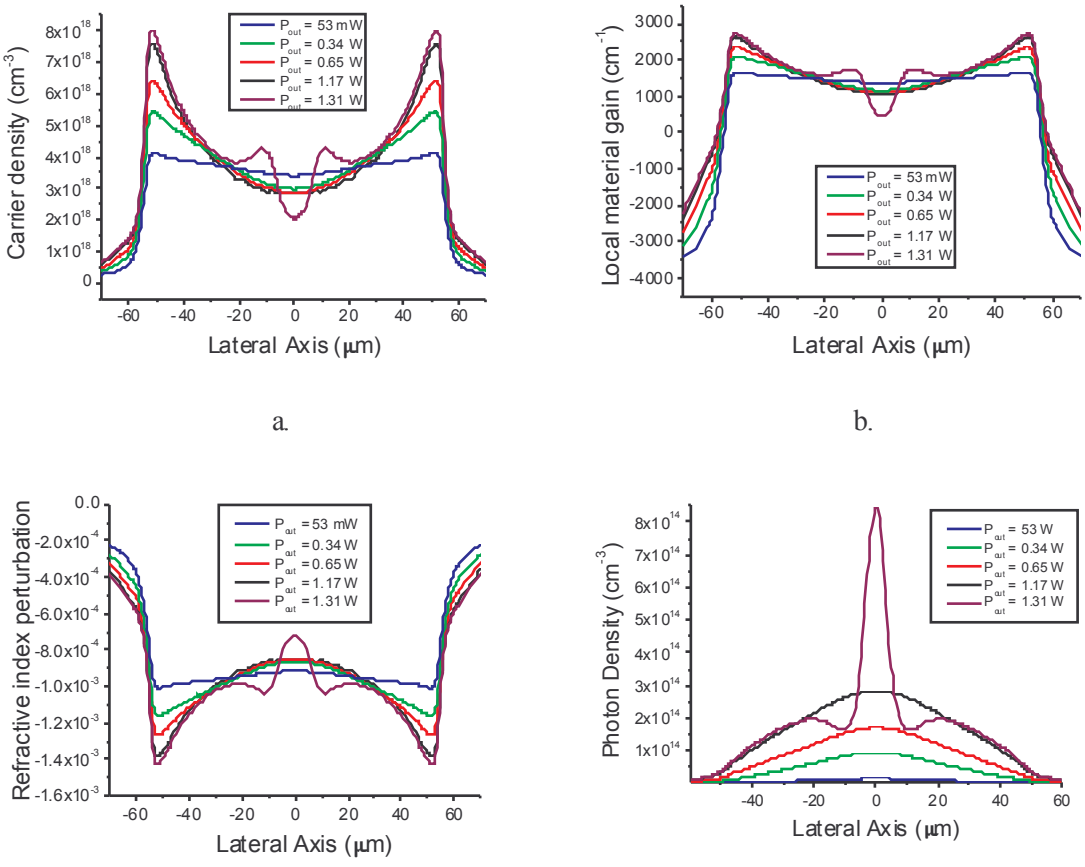

Fig. 9: Carrier density (a), gain (b), index perturbation (c) and photon density (d) profiles at the output facet for the GG tapered laser at different output powers.

3. Performance limits

3.1 Spatial hole burning and self-focusing: Gain Guided Tapered Lasers with beam spoilers

The nearly ideal behaviour of a tapered laser observed at low power changes dramatically when increasing the output power. The main reason is the shape of the optical mode, with a higher photon density in the cavity axis, which depletes the carrier density due to the higher stimulated recombination in this region, the so-called Spatial Hole Burning (SHB) effect. Fig. 9a shows the simulated carrier density for the GG device of section 2 at the output facet for increasing output powers. The carrier density takes a "rabbit-ears" shape, with maxima at the sides and minimum at the center. The carrier density minimum is limited by the transparency carrier density, $1.6 \cdot 10^{18}$ cm^{-3} in our example. The simplified approach by Walpole in [1] suggests that the gain saturation caused by the SHB would induce an increase of the photon density in the side regions, leading to a top hat shape.

But in semiconductor materials a change of the carrier density produces simultaneously changes in the gain and in the refractive index, which are related by the linewidth enhancement factor or α parameter [29]. Figs. 9b) and 9c) show the corresponding gain and index profiles at the power levels of Fig. 9a). The gain decreases at the cavity axis and the refractive index increases. The shape of the index profile produces a parasitic waveguide for the beam, with more important consequences on the beam shape than the gain profile. The carrier induced waveguide produces a convergent lens effect during the propagation along the tapered region, which concentrates the power density at the center of the beam (see Fig. 9 d). The new beam shape further increases the SHB and strengthening the parasitic waveguide. At a given power density, the strong feedback induces self-focusing of the beam, leading to saturation of the output power.

The SHB and self-focusing of the beam not only limit the maximum power, but also degrade the beam quality when increasing the output power: the carrier induced convergent lens narrows the FF divergence and broadens the width of the virtual source (Fig. 10), induces a wandering astigmatism and increases the value of M^2 (Fig.11) Unfortunately, there is not an easy strategy for counteracting SHB and self-focusing, although different ideas have been proposed. The onset of self-focusing can be delayed by using active materials with a reduced α parameter [30, 31] and epitaxial designs with reduced confinement factor Γ [32], or with increased d_w/Γ (d_w is the active layer thickness) [33]. A patterned injection profile matching the shape of the optical mode has been demonstrated experimentally [34, 35] and by mean of simulations [36] to be a promising strategy to improve beam quality. It is clear that further improvements are still possible by optimising the material quality and device geometry.

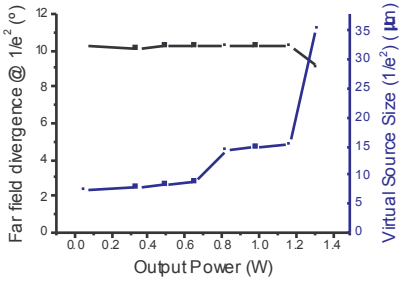

Fig. 10: Evolution of the FF angular width and virtual source size for the GG tapered laser described in text.

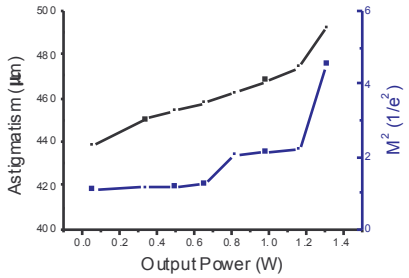

Fig. 11: Evolution of the astigmatism and beam quality parameter M^2 for the GG tapered laser described in text.

3.2 Lack of spatial filtering: GG device without beam spoilers

The optical pumping phenomenon is found to cause a deterioration of the modal filtering efficiency of the ridge waveguide section. With the onset of optical bleaching, the light scattered during back propagation can propagate to the rear facet, where it is reflected and can reach the tapered section. When this unfiltered light reaches the tapered amplifier, it can seed the formation of filaments. Fig. 12a shows the photon distribution at the front facet of the cavity, for a GG tapered diode emitting at 735 nm, with a full taper angle of 4º and without beam spoilers (see refs. [5] and [22] for geometrical details), at output powers of 0.2 W and 2 W. The relative sizes of the side lobes are much smaller at 0.2 W than at 2 W, showing that the filtering efficiency decreases with increasing output power. To investigate this phenomenon in more detail the gain distribution at the rear facet of this device is shown in Fig. 12b. The intensity of the scattered light in the regions adjacent to the ridge waveguide increases with increasing output power, providing optical pumping, which increases the local carrier density and the region outside of the ridge waveguide approaches transparency. As a consequence there is a strong decrease in the filtering efficiency of the straight section

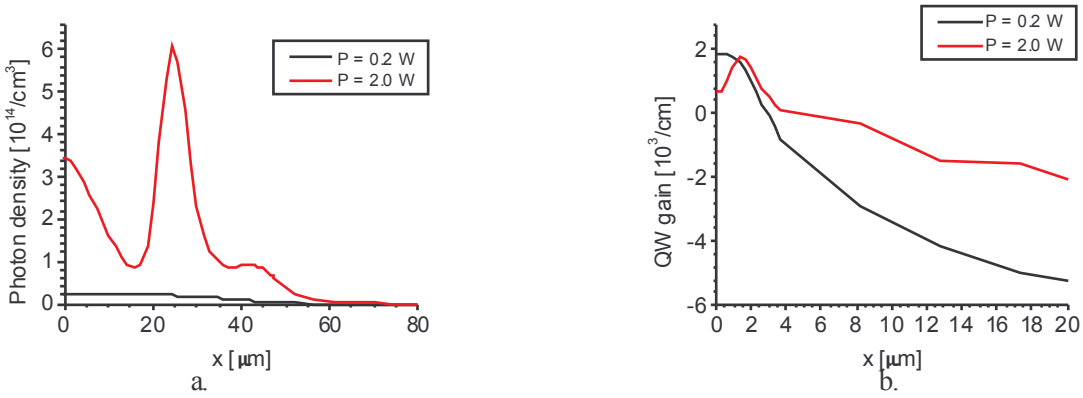

Fig. 12: Simulated photon density distribution at the front facet a) and the gain distribution at the rear facet b) for the laser cavity operating at 735 nm.

The role of the regions adjacent to the ridge waveguide can be understood in more detail as follows (see Fig.13). The backward propagating wave is scattered by the tapered structure, because of its curved phase front (which causes it to diverge). This scattering is particularly significant at the interface between the tapered and straight sections. Consequently, a significant amount of the power in the backward propagating wave is contained in higher order lateral modes, which pumps the electrically un-pumped regions. After reflection at the rear facet, the amplified backward propagating wave seeds the forward propagating wave. The side lobes propagate along the outside of the ridge waveguide and re-enter the electrically pumped region in the tapered section. Thus, if the angle of propagation of the side lobes is smaller than the taper angle they partly scatter from the taper, because the refractive index perturbation forms an anti-guiding structure and form side lobes in the near field patterns and help seed the filamentation process. Consequently, the optical pumping effect triggers spatial hole burning effects and ultimately filamentation.

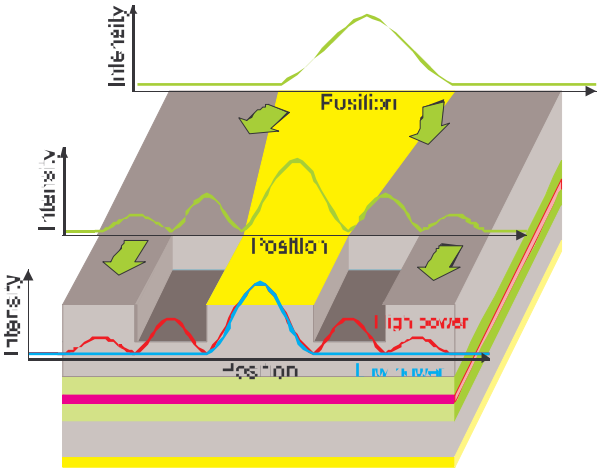

Fig. 13: Schematic illustration of optical pumping in tapered laser diodes

3.3 Narrow angle Index Guided tapered Lasers

The main effect degrading the beam quality of IG tapered lasers is carrier induced lensing and self-focusing, similar to the effect analyzed in section 3.2 for GG devices, but with important differences. The carrier lensing reduces the width of the beam at the output facet down to sizes for which diffraction effects become relevant. Consequently, the angular width of the FF patterns increases with the output power. On the other side, the carrier lensing produces an almost collimated beam inside the cavity, with an apparent virtual source at the output facet. Figs. 14 and 15 show the evolution of the main beam parameters (FF angle, VS size, astigmatism, and M^2) as a function of the output power for the IG device taken as example in section 2. It has been experimentally observed [37] that in some cases the convergent lens effect produced by the SHB can even focus the beam externally to the cavity, yielding a negative value for the astigmatism. Fig. 16 illustrates this effect for a 2.5 mm device at high power. The evolution of the beam inside the tapered region shown in Fig. 16 resembles that of a graded-index lens or optical fiber, due to the graded index carrier induced profile in the tapered region. The strong SHB at high power produces a self-focusing of the beam leading to saturation of the output power.

A novel IG tapered laser design, called the clarinet laser, was recently proposed to obtain a low a stable beam divergence, together with a negligible astigmatism at high power [23]. The idea behind it is to balance the two mechanisms modifying the FF divergence which lead to a decreasing beam divergence with power in GG tapered lasers (see Fig. 10) and to an increasing beam divergence in narrow IG tapered devices (see Fig. 12). This is illustrated in Fig. 17, where we have plotted the simulated evolution of the beam divergence (measured at $1/e^2$) for index guided tapered lasers with different taper angles and a constant output aperture. For this particular active material and emission wavelength, the simulations predict a low and stable beam divergence in the case of a taper angle of 2º. Based on the above theoretical results, a clarinet laser with a relatively long RW section and a relatively short tapered section was fabricated and characterized. The experimental results [23] confirmed the improved stability of the beam divergence when increasing the power in this new design.

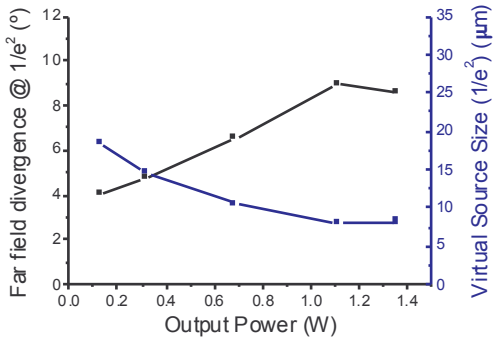

Fig. 14: Evolution of the FF angular width and virtual source size for the IG tapered laser described in text.

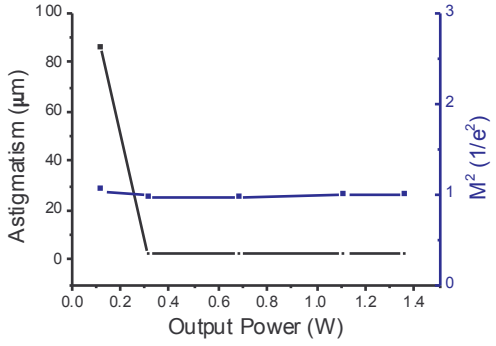

Fig. 15: Evolution of the astigmatism and beam quality parameter M^2 for the IG tapered laser described in text.

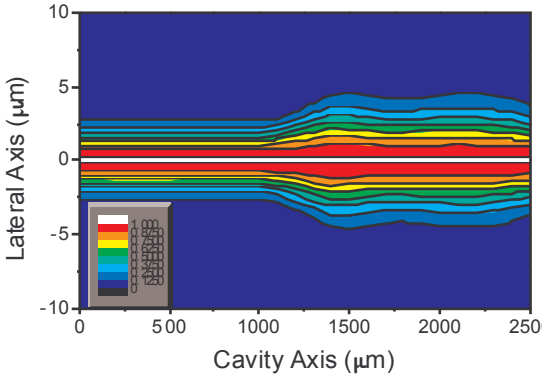

Fig. 16: Normalized forward optical field intensity inside the cavity for a 2.5 mm IG tapered laser operating at high power.

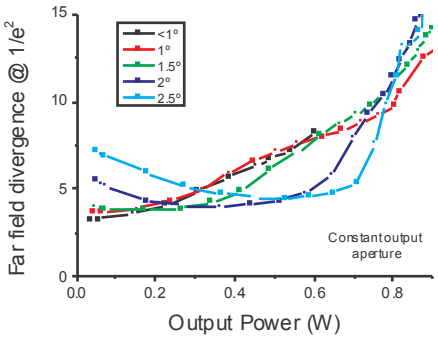

Fig. 17: Evolution of the FF angular width for IG tapered lasers with different taper angles and a constant output aperture.

Summary

Tapered semiconductor lasers are attracting increasing attention due to their commercial potential as reliable, low-cost high brightness optical sources. The performance of tapered lasers is critically dependent upon the optimisation of their structural design. This paper presents a general overview of the key operating principles of high brightness tapered lasers, in order to convey an understanding of main physical phenomena governing the interactions between photons and carriers. The authors provide examples based on simulations which illustrating the ideal operation of tapered lasers with both gain-guided and index-guided tapered regions at low output powers. Further examples are provided for high-power operation to illustrate main physical phenomena, which limit the performance of tapered lasers. Finally, the importance of spatial filtering with a beam spoiling aperture is also demonstrated.

Acknowledgments

The authors gratefully acknowledge M. Krakowski, S. Auzanneau, M. Calligaro, O. Parillaud, and N. Michel (Alcatel-Thales III-V Labs), H. Wenzel, B. Sumpf and G. Erbert (Ferdinand-Braun-Institut für Höchstfrequenztechnik), for providing experimental results on tapered lasers during EC projects "ULTRABRIGHT" and "WWW. BRIGHT.EU". The help provided by M. Keleman (Fraunhofer-Institute for Angewandte Festkörperphysik), N. Linder (Osram), B. Sumpf and N. Michel to update tables I and II is also acknowledged, as well as the contributions of T. Benson, P. Sewell and J. Wykes (University of Nottingham), and G. Batko, J. Arias, and B. Romero (Universidad Politécnica de Madrid) to the simulation program used in this work.

References

[1] J. N. Walpole, "Semiconductor amplifiers and lasers with tapered gain regions," *Opt. Quantum Electron.*, vol. 28, pp. 623-645, 1996.
[2] H. Wenzel, B. Sumpf, G. Erbert, "High-brightness diode lasers," *C. R. Physique*, vol. 4, pp. 649-661, 2003.
[3] E. S. Kintzer, J. N. Walpole, S. R. Chinn, C. A. Wang, L. J. Missaggia, "High-power, strained-layer amplifiers and lasers with tapered gain regions," *IEEE Photon. Technol. Lett.,* vol. 5, pp. 605-607, 1993.
[4] N. Linder, R Butendeich, C. Karnutsch, W. Schmid, S. Tautz, K. Streubel, S. Rurlander, H. Schweizer, F. Scholz, "900mW continuous wave operation of AlInGaP tapered lasers and superluminescent diodes at 640 nm". *Conference on Lasers and Electro-Optics, 2004 (CLEO)*. vol. 1, 16-21 May 2004.
[5] G. Erbert , J. Fricke, R. Huelsewede, A. Knauer, W. Pittroff, P. Ressel, J. Sebastian, B. Sumpf, H. Wenzel, G. Traenkle, "3 W – high brightness tapered diode lasers at 735nm based on tensile strained GaAsP-QWs". *Proc. SPIE,* vol. 4995, 2003.
[6] F. Dittmar, B. Sumpf, J. Fricke, G. Erbert, G. Tränkle, *"High-power 808 nm tapered diode lasers with nearly diffraction-limited beam quality of M^2 = 1.9 at P = 4.4 W".* IEEE Photon. Technol. Lett., *accepted (2006).*
[7] N. Michel, I. Hassiaoui, M. Calligaro, M. Lecomte, O. Parillaud, M. Krakowski, L. Borruel, J. M. García-Tijero, I. Esquivias, S. Sujecki, E. C. Larkins, "High-power diode lasers with an Al-free active region at 915 nm". *Proc. SPIE,* vol. 5989, 2005.
[8] M. T. Kelemen, F. Rinner, J. Rogg, N. Wiedmann, R. Kiefer, M. Walther, M. Mikulla, G. Weimann, "High-power high-brightness ridge-waveguide tapered diode lasers at 940 nm", *Proc. SPIE,* vol. 4648, pp. 75-81, 2002.
[9] M. T. Kelemen, J. Weber, G. Bihlmann, R. Moritz, M. Mikulla, G. Weimann, "Tapered diode lasers at 976 nm with 8 W nearly diffraction limited output power". *Electron. Lett.,* vol. 41, no. 18, p. 1011-13, 2005.
[10] N. Michel, M. Calligaro, M. Krakowski, S. Deubert, J. P. Reithmaier, A. Forchel, "980nm small aperture tapered laser (1W cw, M^2~3) and tapered arrays (>3W cw): comparison between GaInAs/(Al)GaAs quantum dot and quantum well structures". *Proc. SPIE*, vol. 5738, pp. 355-364, 2005.
[11] K. Paschke, B. Sumpf, F. Dittmar, G. Erbert, J. Fricke, A. Ginolas, Ch. Dzionk, A. Knauer, H. Wenzel, G. Tränkle, "5.3 W CW high brightness 980–nm tapered diode lasers". *Conference on Lasers and Electro-Optics, 2005 (CLEO),* pp. 113, 12-17 June 2005.
[12] M.T. Kelemen, J. Weber, F. Rinner, J. Rogg, M. Mikulla, and G. Weimann, "High-brightness 1040-nm tapered diode lasers", *Proc. SPIE,* vol. 4947, pp. 252-260, 2003.
[13] J. N. Walpole, J. P. Donelly, S. H. Groves, L. J. Missagia, J. D. Woodhouse, R. J. Bailey, A. Napoleone, " Diffraction-Limited 1.3-μm-Wavelength Tapered-Gain-Region Lasers With >1-W CW Output Power", ". *IEEE Photon. Technol. Lett.*, vol. 8, pp. 1429-1431, 1996.
[14] S. Kallenbach, M. T. Kelemen, R. Aidam, R. Lösch, G. Kaufel, M. Mikulla, G. Weimann, "High-power high-brightness ridge-waveguide tapered diode lasers at 14xx nm", *Proc. SPIE,* vol. 5738, paper 47, 2005.
[15] S. Delépine, F. Gérard, A. Pinquier, T. Fillion, J. Pasquier, D. Locatelli, J.P. Chardon, H.K. Bissessur, N. Bouché, F. R. Boubal, P. Salet, "How to launch 1W into single-mode fiber from a single 1.48 μm Flared Resonator". *IEEE J. Select. Topics Quantum Electron.*, vol. 7, pp. 111-123, 2001.
[16] J. Wagner, E. Geerlings, G. Kaufel, M. T. Kelemen, C. Manz, C. Pfahler, M. Rattunde, J. Schmitz, "(AlGaIn)(AsSb) quantum well diode lasers with improved beam quality", *Proc. SPIE,* vol. 5732, paper 82, 2005.
[17] S. Auzanneau, M. Krakowski, F. Berlie, M. Calligaro, Y. Robert, O. Parillaud, M. Lecomte, B. Boulant, T. Fillardet, "High-power and high-brightness laser diode structures at 980 nm using an Al-free active region". *Proc. SPIE,* vol. 4995, pp. 184-195, 2003.
[18] M. Mikulla, A. Schmitt, M. Walther, R. Kiefer, W. Pletschen, J. Braunstein, and G. Weimann, "25-W high-brightness tapered semiconductor laser-array". *IEEE Photon. Technol. Lett.*, vol. 11, pp. 412-414, 1999.

[19] F. J. Wilson, J. J. Lewandowski, B. K. Nayar, D. J. Robbins, P. J. Williams, N. Carr, F.O. Robson, "9.5W cw output power from high brightness 980 nm InGaAs/AlGaAs tapered laser arrays". *Electron. Lett.,* vol. 35, pp. 43-45, 1999.

[20] P. J. Williams, J. J. Lewandowski, D. J. Robbins, A. K. Wood, F. O. Robson, B.K. Nayar, "Tapered laser arrays for high power operation (>1.4 W cw) at 1.59 µm for applications in surgery". *Electron. Lett.,* vol. 34, pp. 993-994, 1998.

[21] L. Borruel, S. Sujecki, P. Moreno, J.Wykes, M. Krakowski, B. Sumpf, P. Sewell, S. C. Auzanneau, H. Wenzel, D. Rodríguez, T. M. Benson, E. C. Larkins, I. Esquivias, "Quasi-3-D Simulation of High-Brightness Tapered Lasers". *IEEE J. Quantum Electron.,* vol. 40, pp. 463-472, 2004.

[22] S. Sujecki, L. Borruel, J. Wykes, P. Moreno, B. Sumpf, P. Sewell, H. Wenzel, T. M. Benson, G. Erbert, I. Esquivias, E. C. Larkins, "Nonlinear Properties of Tapered Laser Cavities". *IEEE J. Select. Topics Quantum Electron.,* vol. 9, pp. 823-834, 2003.

[23] L. Borruel, I. Esquivias, P.Moreno, M. Krakowski, S. C. Auzanneau, M, Calligaro, O. Parillaud, M. Lecomte, S. Sujecki, J. Wykes, E. C. Larkins, "Clarinet laser: Semiconductor laser design for high-brightness applications". *Appl. Phys. Lett.*, vol 87, 2005.

[24] K. A. Williams, R. V. Penty, I. H. White, D. J. Robbins, F. J. Wilson, J. J. Lewandowski, B. K. Nayar, "Design of High-Brightness Tapered Laser Arrays", *IEEE J. Select. Topics Quantum Electron.,* vol 5, pp. 822-831, 1999.

[25] S. Mariojouls, S. Margott, A. Schmitt, M. Mikulla, J. Braunstein, G. Weimann, F. Lozes, S. Bonnefont, " Modeling of the Performance of High-Brightness Tapered Lasers". *Proc. SPIE*, vol. 3944, pp. 395-406, 2000.

[26] H. Odriozola, L. Borruel, J.M.G. Tijero, I. Esquivias, S. Sujecki, E.C. Larkins, "Losses of the unstable cavity in tapered laser diodes: estimation from numerical simulations", *Proceedings of the 5th International Conference on Numerical Simulation of Optoelectronic Devices, 2005, (NUSOD '05),* pp 31–32, 19-22 Sept. 2005.

[27] M. Krakowski, S. C. Auzanneau, M. Calligaro, O. Parillaud, P. Collot, M. Lecomte, B. Boulant, T. Fillardet, "High power and high brightness laser diode structures at 980 nm using Al-free materials", *Proc. SPIE*, vol. 4651, pp. 80-91, 2002.

[28] International Organization of Standardization, ISO11146.

[29] C. H. Henry, "Theory of the linewidth of semiconductor lasers," *IEEE J. Quantum Electron.*, vol. 18, pp. 259-264, Feb. 1982.

[30] J. G. McInerney, P. O'Brien, P. Skovgaard, M. Mullane, J. Houlihan, E. O'Neill, J. V. Moloney, R. A. Indik,"Towards filament-free semiconductor lasers", *Proc. SPIE*, vol. 3944, pp. 375-386, 2000.

[31] L. Borruel, S. Sujecki, D. Rodríguez, J. Wykes, M. Krakowski, P. Moreno, P. Sewell, T. M. Benson, E. C. Larkins, I. Esquivias; "Beam filamentation and maximum optical power in high brightness tapered lasers". *Proc. SPIE,* vol. 4986, pp. 423-431, 2003.

[32] M. Mikulla, P.Chazan, A. Schmitt, S. Morgott, A. Wetzel, M. Walther, R. Kiefer, W. Pletschen, J. Braunstein, G. Weimann, "High–brightness tapered semiconductor laser oscillators and amplifiers with low-modal gain epilayer structures," *IEEE Photon. Technol. Lett*., vol. 10, pp. 654-656, 1998.

[33] J. M. G. Tijero, D. Rodríguez, L. Borruel, S. Sujecki, E. C. Larkins, I. Esquivias, "Optimization of epitaxial layer design for high brightness tapered lasers", *Proc. SPIE* , vol. 5722, pp. 280-287, 2005.

[34] P. Salet, F. Gérard, T. Fillion, A. Pinquier, J. L. Gentner, S. Delépine, P. Doussière, "1.1-W continuous-wave 1480-nm semiconductor lasers with distributed electrodes for mode shaping," *IEEE Photon. Technol. Lett.*, vol. 10, pp. 1706–1708, 1998.

[35] J. N. Walpole, J. P. Donnelly, L. J. Missaggia, Z. L. Liau, S. R. Chinn, S. H. Groves, P. J. Taylor, M.W. Wright, "Gaussian patterned contacts for improved beam stability of 1.55-µm tapered lasers," *IEEE Photon. Technol. Lett.*, vol. 12, pp. 257–259, 2000.

[36] L. Borruel, S. Sujecki, P. Moreno, J. Wykes, P.Sewell, T. M Benson, E. C. Larkins, I. Esquivias, "Modeling of Patterned Contacts in Tapered Lasers", *IEEE J. Quantum Electron.*, vol. 40, pp. 1384-1388, 2004.

[37] N. Michel. Private Communication.